X-ray absorption in perfect crystals

by

John David Zimmerman

A Thesis Submitted to the

Graduate Faculty in Partial Fulfillment of the

Requirements for the Degree of

MASTER OF SCIENCE

Department: Physics

Major: Solid State Physics

Iowa State University
Ames, Iowa

1984

TABLE OF CONTENTS

LIST OF FIGURES

Page

LIST OF TABLES

CHAPTER 1

Introduction

When a beam of photons or particles such as neutrons impinges on the surface of a material, transmission of the beam can always be observed by changing the nature of the material or by modifying the magnitude of the wavelength of the beam. The shorter the wavelength is, the more the beam will penetrate the material. A second phenomenon will also occur: scattering of the beam due to diffraction.

Diffraction in amorphous materials, liquids and gases produces intensity distributions from which one may calculate the so-called "radial distribution function" (Hosemann and Bagchi, 1962). Figure 1.1(i) curve (a) illustrates the experimental intensity curve for liquid sodium as a function of $(\sin \theta)/\lambda$. Curve (b) shows the total independent scattering assuming a completely random arrangement of atoms. Curves (c) and (d) show the correction for incoherent radiation. Figure 1.1(ii) curve (a) shows the radial distribution function for liquid sodium which is calculated from information in Figure 1.1(i). The average radial density curve $4\pi r^2 \rho_o$ (curve b), and the distribution of neighbors in crystalline sodium (curve c) are also shown in Figure 1.1(ii). From the radial distribution function it is possible to calculate the number of neighboring atoms as a function of distance.

Diffraction of x-rays by the lattice planes in a crystal occurs when the Bragg condition is satisfied (see Figure 1.3). That is when

(i) (a) Corrected experimental intensity curve for liquid sodium in electron units per atom. (b) Total independent scattering per atom. (c) Independent coherent scattering per atom. (d) Incoherent scattering per atom

(ii) (a) Radial distribution curve for liquid sodium. (b) Average density curve. (c) Distribution of neighbors in crystalline sodium

Figure 1.1. Experimental intensity curve and radial distribution function for liquid sodium (Tarosov and Warren, 1936)

(i)

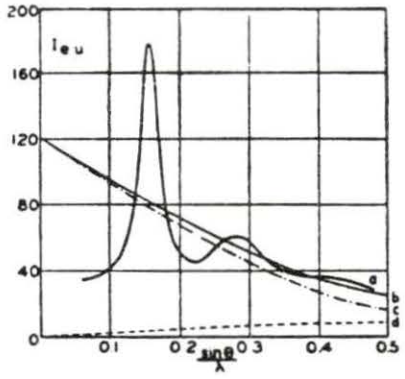
200
160
120
80
40
0
I_{eu}
0·1
0·2
0·3
0·4
0·5
$\frac{\sin\theta}{\lambda}$
a
b
c
d

(ii)

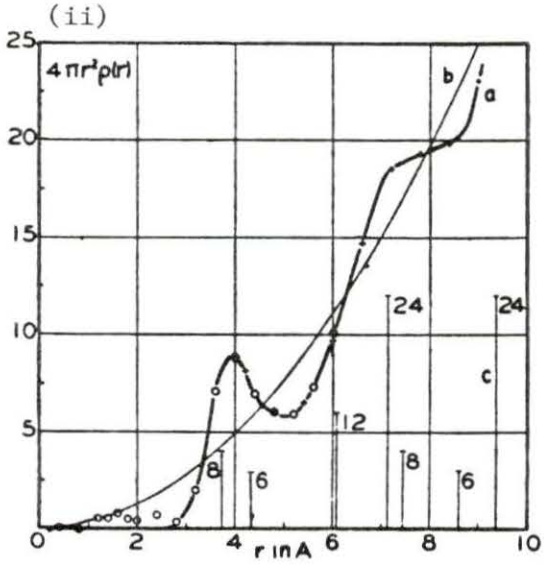
25
20
15
10
5
0
$4\pi r^2\rho(r)$
b
a
24
24
c
12
8
6
8
6
2
4
r in A
6
8
10

$$\lambda = 2d_{hkl} \sin\theta_{hkl} \tag{1.1}$$

where λ is the wavelength, d is the spacings between atomic planes, θ is the diffraction or Bragg angle with respect to the atomic planes and h, k and l are the Miller indicies of the atomic planes.

Diffraction by various atomic planes for single and poly-crystalline samples allows one to determine crystal structures when the structure factors are known. Structure factors, F_{hkl}, are determined from the relation (see, for instance, Arndt and Willis, 1966)

$$I_{hkl} = kLp\lambda^3 \left|F_{hkl}\right|^2 \tag{1.2}$$

where n = 1 for perfect crystals, n = 2 for ideally mosaic crystals, λ is the wavelength of the incident beam, p the polarization factor which is n dependent, L the Lorentz factor, k the scale factor containing among other things the attenuation and extinction effects, I the intensity of a Bragg peak and h, k and l are the Miller indicies of the Bragg reflections. The accuracy of the structure factor depends upon the accuracy of all the parameters mentioned above. It is evident that proper attenuation corrections are of fundamental importance, as it will be shown below, in the determination of accurate structure factors. These structure factors may lead to the determination of electron charge density distributions.

In this study, it has been found that the linear attenuation coefficients in the regime of thick crystals or small angles is much different than those found for thin crystals or large angles. The latter are comparable to attenuation coefficients previously published (see,

Figure 1.2. Intensity versus thickness of a transmitted x-ray beam

Figure 1.3. Processes of x-rays passing through a crystal. (Note that there are three processes presented: diffraction, refraction, and transmission)

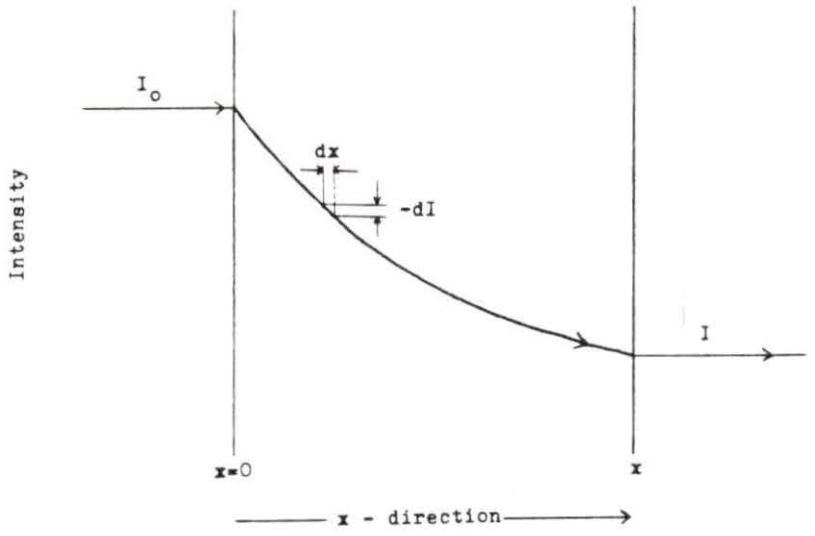
Intensity
I_o
dx
-dI
I
x=0
x
x - direction

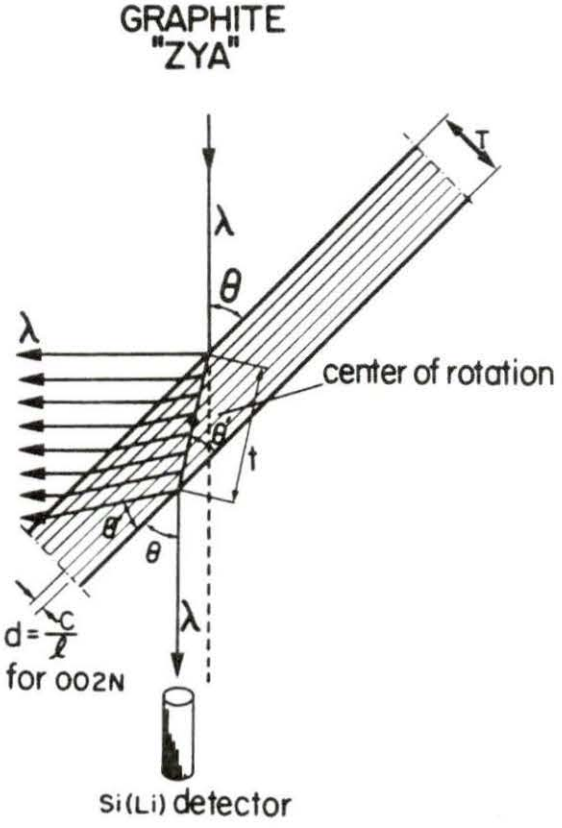
GRAPHITE
"ZYA"
λ
θ
λ
center of rotation
t
θ
θ
θ
λ
$d=\frac{c}{\ell}$
for 002N
Si(Li) detector

for example, International Tables for X-ray Crystallography, 1974). This has a profound effect on any calculations for which electron charge density distributions are done since these studies essentially rely on data for which the scattering angle is small. In this regime the attenuation coefficients may not necessarily be those which have been published. This means that attenuation coefficients should be measured before intensity determination takes place.

Transmission and attenuation

When a beam of monochromatic x-rays passes through a thin layer of matter, the fraction of the intensity, dI/I, absorbed or attenuated by the material is proportional to the thickness of the layer dx. This is expressed by the equation

$$dI/I = -\mu dx \tag{1.3}$$

in which the proportionality constant μ is known as the linear attenuation coefficient (Schwartz and Cohen, 1977). The negative sign indicates a decrease in the intensity of the transmitted beam. If μ is really a constant in the distance and also in intensity then equation 1.3 may be integrated to give

$$I = I_o \exp(-\mu x) \tag{1.4}$$

where I_o is the intensity of the beam at x = o, and I the intensity of the transmitted beam at x. Figure 1.2 illustrates the relationships of the intensities of Equations 1.3 and 1.4.

In general, the average absorption coefficient μ_o of a single crystal is made up of three different contributions (Pinsker, 1978):

$$\mu_o = \mu_{PE} + \mu_{TDS} + \mu_C. \tag{1.5}$$

The first contribution which accounts for more than 90% of the total average attenuation coefficient is due to the photoelectric effect. The second contribution is due to "Thermal Diffuse Scattering"; it is a coherent scattering process produced by phonons. The third contribution is due to incoherent or Compton scattering. There are other contributions to the total attenuation coefficient (Grodstein, 1957). The scope of this work, however, is limited to the above three contributions.

A method for measuring attenuation coefficients

The transmission method used in this study, involves rotating a crystal wafer in a beam of monochromatic x-rays and measuring the intensity of the transmitted beam. This process is represented in Figure 1.4. Because the beam path length through the crystal changes as the crystal is rotated, Equation 1. may be used to calculate the attenuation coefficient. This transmission method has the advantage that only the crystal is rotated. The detector is constantly set in the line of sight of the direct beam. Thus, any errors due to detector misalignment are eliminated. In this study the spatial distribution of the beam behind the crystal was not examined, however the detector collimator was wide open for all scans.

Materials studied

The crystals used in this study are germanium, silicon and highly oriented pyrolytic graphite (HOPG). Germanium and silicon are cubic while graphite is hexagonal (Kittel, 1971). Characterization of these crystals is important because these materials have properties which are useful for other types of studies (Schwartz and Cohen, 1977). To this day, germanium and silicon are the most perfect crystals that can be produced. They are well suited as materials for x-ray or neutron interferometers or as monochromator crystals where the transmission bandwidth must be narrow. HOPG (Union Carbide, grade ZYA) almost behaves as a perfect crystal along the c-axis while the atoms in the basal planes are more or less randomly distributed. Because of the randomness in the basal plane, HOPG cannot be considered as an ideally mosaic crystal.

This arrangement of atomic planes makes HOPG an ideal monochromator crystal because these planes are highly reflective under the Bragg condition. The intensities from these reflections in HOPG are much higher than those from reflections of silicon or germanium. The disadvantage of using HOPG is that the bandwidth of a monochromator made from such a crystal is much larger than that of either silicon or germanium.

Example: Bonse-Hart Camera

The Bonse-Hart Camera is a device made from a single silicon crystal in which a rectangular groove or channel has been cut in a particular orientation with respect to a crystallographic axis. It is used like a monochromator crystal. Through multiple reflections within the channel,

it narrows the distribution of the direct beam. Therefore, this device dramatically improves the resolution of small angle diffraction. When taking into account dynamical effects, regular attenuation and other processes which may determine the final intensity profile of the diffraction peak, it has been found that the center of the profile fits theoretical calculations while the tails of the distribution are much higher by an order of magnitude as compared to theoretical profiles. As mentioned previously, the attenuation coefficients used to calculate intensities in this regime of small angle scattering, which the Bonse-Hart Camera operates in, may not necessarily be the ones which are published in the tables.

Outline of the present work

Attenuation coefficients for the elements have been measured for many of the standard wavelengths (Grodstein, 1957). Calculations for these have also been compiled (Grodstein, 1957; McGinnies, 1959; International Tables for X-ray Crystallography, 1974). In this study, attenuation coefficients for germanium, silicon and HOPG are measured for the fundamental, second and third harmonic wavelengths of the tungsten Ll, $L\alpha_1$, $L\beta_1$, and $L\gamma$, excitation lines. Table 1.1 contains a list of the excitation lines and harmonic wavelengths used in this study.

Presently, the relation between the atomic scattering factor and the photoelectric contribution to the attenuation coefficient will be discussed. Also, theoretical calculations of these will be discussed along with theoretical calculations for the coherent and incoherent

processes. Following this, the unique apparatus on which the experiment was performed along with some general experimental techniques which were used will be described. This is proceeded by the results and discussion of the data obtained for the perfect crystals and HOPG. Also, experimental attenuation coefficients for HOPG are presented for different temperatures. Within the conclusions, the results of the data are summarized and differences in obtaining attenuation coefficients for the perfect crystals and HOPG are discussed. In the final chapter, recommendations are given for further studies to determine characteristics of the change of the linear attenuation coefficient in the regime of the thick crystal or small scattering angle.

Table 1.1. Excitation lines of tungsten and other wavelengths used in this study

Excitation Line	λ(Å)	$\lambda/2$(Å) Bremsstrahlung	$\lambda/3$(Å) Bremsstrahlung
L_1	1.6782	0.8391	0.5594
$L\alpha_1$	1.47639	0.73819	0.49213
$L\beta_1$	1.28181	0.64091	0.42727
$L\gamma_1$	1.09855	0.54928	0.36618

CHAPTER 2

Theory

The theoretical treatment of the photoelectric attenuation coefficient as given by James (1982) will be summarized. For a single atomic species, it is customary to write the atomic scattering factor as

$$f = f_o + \Delta f' + i\Delta f''. \tag{2.1}$$

where the $\Delta f'$ and $\Delta f''$ are the Hönl or anomalous dispersion corrections and are dependent on the frequency of the incident radiation. f_o is the form factor depending on charge distribution and is independent of frequency. If the incident frequency is not too close to an absorption edge, oscillator damping may be neglected. Then $\Delta f'$ is given by

$$\Delta f' = \sum_j \int_{\omega_j}^{\infty} \frac{\omega^2 (dg/d\omega)_j}{\omega_i^2 - \omega^2} \, d\omega \tag{2.2}$$

where the summation is over all the absorption edges and $(dg/d\omega)_j$ is the oscillator density of electron j at frequency ω, $(dg/d\omega)_j d\omega$ the number of virtual oscillators having frequencies between ω and $\omega + d\omega$, ω_i the incident frequency, ω_j the frequency of the absorption edge.

The imaginary component, $\Delta f''$, is given by

$$\Delta f'' = \frac{\pi}{2} \omega_i \sum_j (dg/d\omega)_j \tag{2.3}$$

where the summation is again over all the absorption edges.

It is possible to relate the oscillator density functions $(dg/d\omega)_j$ to the photoelectric attenuation coefficients.

The refractive index of x-rays is related to the atomic scattering factor by

$$n = 1 - \delta = 1 - \frac{\lambda^2 e^2 N f}{2\pi mc^2} \tag{2.4}$$

where n is the index of refraction, λ the wavelength, e the charge of the electron, c the speed of light, N the number of atoms per unit volume and f is the atomic scattering factor in the forward momentum direction. Substituting Equation 2.1 into Equation 2.4, it is evident that the refractive index is complex. The equation obtained is

$$n = 1 - \frac{\lambda^2 e^2 N}{2\pi mc^2} (f_o + \Delta f') - i \left(\frac{\lambda^2 e^2 N}{2\pi mc^2} \right) \Delta f'' \tag{2.5}$$

Suppose now that a wave is traveling in a direction x in a medium whose refractive index is n. Then to get a displacement at x, given the displacement at x = 0, we have to multiply the wave by a phase

$$\Phi = \exp(-iknx) \tag{2.6}$$

where $k = 2\pi/\lambda$. Substituting Equation 2.5 into 2.6, the phase may be separated into two parts:

$$\Phi = \exp(-\alpha \Delta f'' kx) \exp(-ikx(1-\alpha(f_o + \Delta f'))) \tag{2.7}$$

where $\alpha = \lambda^2 e^2 N / 2\pi mc^2$.

The second term in this product corresponds to a phase lag and is due to the real part of n. The first term causes the displacement to decrease exponentially as a function of x. Thus this term, due to the imaginary part of n, corresponds to an attenuation. Since the ordinary linear attenuation coefficient refers to intensity and not amplitude, μ may be written as

$$\mu = 2\alpha k \Delta f'' \tag{2.8}$$

Substituting for α and using the relation $\omega = 2\pi/\lambda$, μ is related to the scattering factor by

$$\mu_j(\omega_i) = \frac{4\pi e^2}{m\omega_i c} \Delta f_j'' \tag{2.9}$$

where $\mu_j(\omega_i)$ is the atomic attenuation coefficient for the jth atomic shell and $\mu_j(\omega_i) = 0$ if $\omega < \omega_j$. This is related to the linear attenuation coefficient by $\mu_{j(\text{linear})} = N\mu_j$ where N has already been defined. Summing over the absorption edges, Equation 2.9 becomes

$$\Delta f'' = \sum_j \Delta f_j'' = \sum_j \frac{mc}{4\pi e^2} \omega_i \mu_j(\omega_i) \tag{2.10}$$

where $\Delta f_j'' = 0$ if $\omega < \omega_j$.

Comparing Equation 2.10 and 2.3 the oscillator density may be written as

$$\left(\frac{dg}{d\omega}\right)_j = \frac{mc}{2\pi^2 e^2} \mu_j(\omega) \tag{2.11}$$

The variation of $\mu_j(\omega)$ for a particular edge is fairly well represented by the empirical formula (see James, 1982, p. 147)

$$\mu_j(\omega) = \begin{cases} (\omega_j/\omega)^n \ \mu_j(\omega_j) & \text{for } \omega > \omega_j \\ \\ 0 & \text{for } \omega < \omega_j \end{cases} \tag{2.12}$$

where n is usually some number of order 3. The value of n varies depending on the particular edge involved, and is a function of atomic number.

If n and $\mu_j(\omega_j)$ are determined from experiment, the anomalous contributions to the structure factor may be calculated by substituting Equation 2.11 and 2.12 into 2.2 and 2.3 to obtain

$$\Delta f'_j = \frac{mc}{2\pi^2 e^2} \ \mu_j(\omega_j) \ \omega^n{}_j \int_{\omega_j}^{\infty} \frac{\omega^2 d\omega}{(\omega^2{}_i - \omega^2)\omega^n} \tag{2.13}$$

$$\Delta f''_j = \frac{mc}{4\pi e^2} \ \omega_i \left(\frac{\omega_j}{\omega_i}\right)^n \ \mu_j(\omega_j). \tag{2.14}$$

Further, the total oscillator strength may be calculated by integration of Equation 2.11 using 2.12. For the total oscillator strength we get

$$g_j = \int_{\omega_j}^{\infty} (dg/d\omega)_j d\omega$$

$$g_j = \frac{mc}{2\pi^2 e^2} \mu_j(\omega_j) \int_{\omega_j}^{\infty} \left(\frac{\omega_j}{\omega}\right)^n d\omega$$

$$g_j = \frac{mc}{2\pi^2 e^2} \left(\frac{\omega_j}{n-1}\right) \mu_j(\omega_j). \qquad (2.15)$$

From Equation 2.11, it is evident that $\mu_j(\omega)$ may be calculated if the oscillator strength is known. Theoretical calculations of $(dg/d\omega)_j$ have been done (Hönl, 1933). By approximating atomic wave functions with hydrogen-like eigenfunctions Hönl, obtained

$$\frac{dg}{d\omega}_K = \frac{2^8 e^{-4}}{9\ \omega_K} \left[\frac{4}{(1 - \delta_K)^2} \left(\frac{\omega_K}{\omega_i}\right)^3 - \frac{1}{(1-\delta_K)^3} \left(\frac{\omega_K}{\omega_i}\right)^4 \right] \qquad (2.16)$$

for the K electrons. Here $\delta_K = 1 - h\omega_K/E_{K,Som}$ where $E_{K,Som}$ is the energy eigenvalue using Sommerfeld's fine structure formula. Hönl also has calculated the oscillator strengths for the L and M electrons. The expressions for these are much more complicated. The equations for the K electrons are quite satisfactory for calculating the associated oscillator strength (Grimvall and Persson, 1969. Cromer, 1965).

However, those equations for the L and M electrons are not as good (Cromer, 1965).

Wagenfeld (1966) has calculated expressions for the atomic photoelectric cross sections for the non-relativistic region. Starting from first principles, an approximation from atomic to hydrogen-like wavefunctions is made for both the bound and free electron states. The hydrogen-like wavefunctions were corrected for inner screening. The retardation factors in the transition probabilities are expanded in a Taylor series which corresponds to an electric multipole expansion. From this, Wagenfeld calculated the attenuation cross sections for the dipole, quadrupole, and octupole transitions. Each was done for electrons in the K, L, and M shells. Refer to Wagenfeld's paper for details of his calculations and the 20 expressions he derived for the absorption cross sections of each electron in the K, L, and M shells.

Theoretical calculations have also been done for the last two terms in Equation 1.5. The contribution due to phonon scattering is made of two parts (Ghezzi et al., 1971):

$$\mu_{TDS} = \mu^{ES} + \mu^{PC} \tag{2.17}$$

μ^{ES} is the scattering contribution calculated by using a model in which the oscillations of the various atoms are independent. Hall and Hirsch (1965) have done calculations to obtain expressions for μ^{ES}. μ^{PC} is the contribution due to pair correlations among the vibrating atoms. A formula for this contribution has been derived by Dederichs (1966). Refer to the above cited papers for derivations of the

expressions mentioned.

Theoretical expressions for the Compton contribution, μ_c, to the absorption coefficient have also been done. (See, for example, Sano, et al., 1969; International Tables for X-ray Crystallography, 1974). The Compton contribution is essentially due to incoherent scattering of x-rays from the outside electrons of the atoms.

CHAPTER 3

Experimental Techniques

Instrumentation

The experimental arrangement is schematically shown in Figure 3.1. The source is a 15 kW Elliott GX-21 rotating anode X-ray generator (60kV and 300mA - only up to 50 kV). The selection of the wavelength is done through a double-monochromator built in Ames to work under helium atmosphere in order to dissipate the heat of the motors and to reduce absorption and diffusion. The crystals under study are mounted in a diffractometer. The diffractometer is a large HUBER triple axis spectrometer with an Eulerian cradle.

The tungsten anode, which was used in this study is water cooled and rotates at 3000 revolutions per minute. Because of high melting temperature of tungsten, this anode can be fully loaded up to 15 kV to take advantage of the intense bremsstrahlung spectrum of tungsten.

The double monochromator provides a wavelength range which can be varied by the computer from about 0.25 to 6 Angstroms; it has the following configuration: two crystal tables rotating independently of each other with a resolution of 1600 steps/degree; the incident crystal table being translated on a motorized slide to satisfy the two Bragg conditions on the two crystals with a resolution of 0.01 mm/step; the three above motions are computerized and, in addition, there are eight other motorized setting motions which can be activated through individual switches.

Figure 3.1. Schematic representation of experimental apparatus

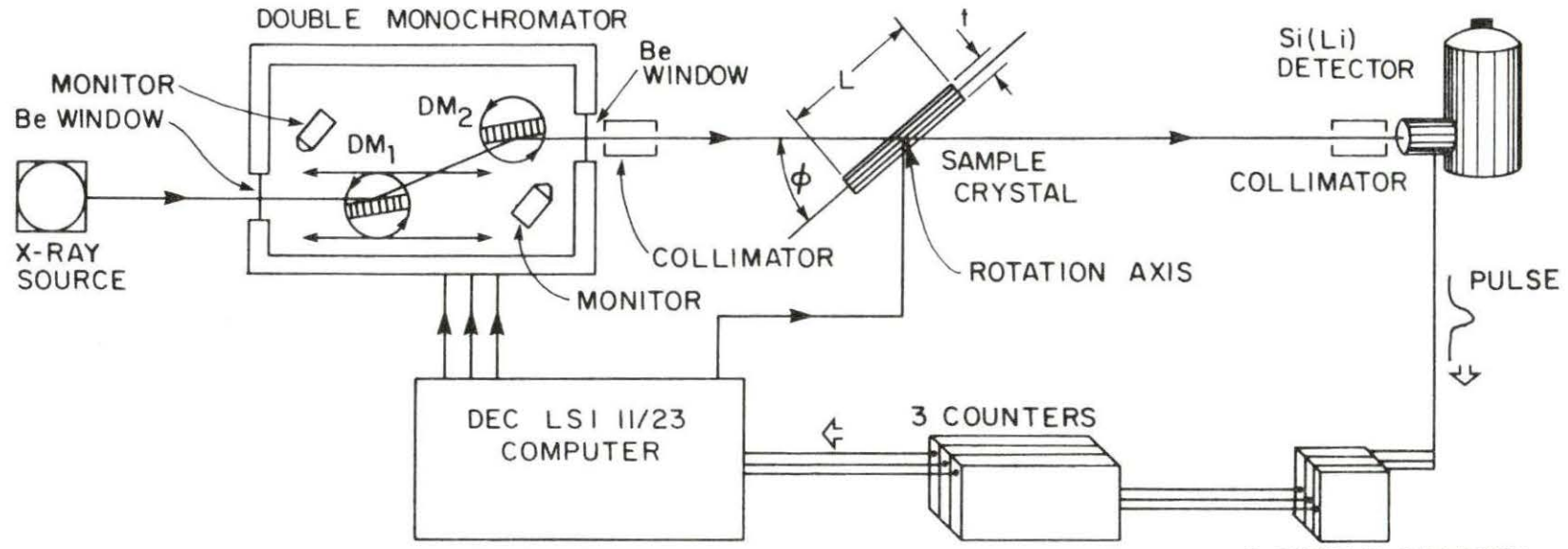

DM_1 DOUBLE MONOCHROMATOR CRYSTAL 1 (HOPG-GRADE ZYB)
DM_2 DOUBLE MONOCHROMATOR CRYSTAL 2 (HOPG-GRADE ZYA)

The positions of the crystal and detector on the diffractometer are also computer controlled. The resolution for the "theta" and "two theta" angles as well as for the rotations controlling the position of the analyzer is 8000 steps/degree. The resolution of the two rotations in the Eulerian cradle is 400 steps/degree. In addition, a helium, closed cycle refrigerator having a temperature range of 6.7 to 400 K can be mounted on the diffractometer.

Monochromator optimization

For comparison purposes, this study requires the knowledge of the wavelength. It is, therefore, easier and more accurate to choose a wavelength which is an excitation line like one of those listed in Table 3.1. These excitation lines show up as strong peaks in the wavelength spectrum of the x-ray source. Figure 3.2 shows these peaks for only part of the spectrum. The background is due to the Bremsstrahlung radiation. By using these peaks which have high intensities the wavelengths can be determined to a high degree of accuracy.

Essentially, the monochromator may be tuned through the application of Bragg's Law ($m\lambda = 2d \sin\theta$) on the monochromator crystals.

The positions of the monochromator crystals (2 rotations and 1 translation as shown in Figure 3.1), have previously been determined by Staudenmann (1984) for the transmission of the Ll, $L\alpha_1$, $L\beta_1$, and $L\gamma_1$ tungsten lines used in this study. The monochromator crystals are driven to a previously determined position depending on the wavelength sought. The crystal positions are then slightly "rocked" about their initial positions. New positions for the crystals are determined by

Table 3.1. Excitation lines of tungsten with associated wavelengths and energies[a]

Excitation Line		Wavelengths (Angstrom)	Error (Angstrom)	Energy (KEV)	Relative Intensity
M ζ_2	$\zeta_2 M_{IV} N_{II}$	8.993	.005	1.3787	.01
M ζ_1	$\zeta_1 M_V N_{III}$	8.962	.004	1.3835	.01
M_4N_3	$M_{IV} N_{III}$	8.573	.008	1.116	.01
M_3N_1	$M_{III} N_I$	7.36	.008	1.684	.5
M_5O_3	$M_V O_{III}$	7.005	.009	1.77	.01
$M\alpha_2$	$\alpha_2 M_V N_{VI}$	6.992	.002	1.7731	100.
$M\alpha_1$	$\alpha_1 M_V N_{VII}$	6.983	.001	1.7754	100.
M_4O_2	$M_{IV} O_{II}$	6.806	.009	1.822	.01
M β	$\beta M_{IV} N_{VI}$	6.757	.001	1.8319	15.
M_2N_1	$M_{II} N_I$	6.28	.02	1.973	.01
M_3N_4	$M_{III} N_{IV}$	6.134	.004	2.021	.1
M γ	$\gamma M_{III} N_V$	6.092	.003	2.035	1.
M_2O_1	$M_{II} O_I$	5.628	.008	2.203	.01
M_2N_4	$M_{II} N_{IV}$	5.357	.004	2.314	.1
M_1N_3	$M_I N_{III}$	5.172	.009	2.397	.5
$M_1O_{2,3}$	$M_I O_{II,III}$	4.44	.02	2.792	.01
L l	$L L_{III} M_I$	1.6782	.0001	7.3878	3.
L T	$T L_{III} M_{II}$	1.6244	.0003	7.632	.01
L S	$S L_{III} M_{III}$	1.5642	.0003	7.926	.01
L α_2	$\alpha_2 L_{III} M_{IV}$	1.48743	.00002	8.3352	10.
L α_1	$\alpha_1 L_{III} M_V$	1.47639	.00002	8.3976	100.

[a]See International Tables for X-ray Crystallography (1974).

Table 3.1. continued

Excitation Line		Wavelength (Angstrom)	Error (Angstrom)	Energy (KEV)	Relative Intensity
L η	$\eta L_{II}M_{I}$	1.4211	.00003	8.7243	1.
L β_{17}	$\beta_{17}L_{II}M_{III}$	1.3387	.0002	9.261	.01
L_1M_1	$L_{I}M_{I}$	1.3365	.0003	9.277	.01
L β_4	$\beta_4L_{I}M_{II}$	1.30162	.00005	9.5252	4.
L β_6	$\beta_6L_{III}N_{I}$	1.28989	.00007	9.6117	.1
L β_1	$\beta_1L_{II}M_{IV}$	1.28181	.000009	9.67235	50.
L_3N_2	$L_{III}N_{II}$	1.2765	.0002	9.712	.01
L_2M_5	$L_{II}M_{V}$	1.2728	.0002	9.741	.01
L_3N_3	$L_{III}N_{III}$	1.2672	.0002	9.784	.01
L β_3	$\beta_3L_{I}M_{III}$	1.26269	.00005	9.8188	6.
L β_{15}	$\beta_{15}L_{III}M_{IV}$	1.24631	.00003	9.9178	1.
L β_2	$\beta_2L_{III}N_{V}$	1.2116	.00003	9.9615	20.
L β_7	$\beta_7L_{III}O_{I}$	1.224	.00004	10.1292	.1
$L_3O_{2,3}$	$L_{III}O_{II,III}$	1.2211	.0002	10.153	.01
L U	U $L_{III}N_{VI,VII}$	1.21868	.00005	10.1733	.01
L β_5	$\beta_5L_{III}O_{IV,V}$	1.21545	.00003	10.2004	.1
L β_{10}	$\beta_{10}L_{I}M_{IV}$	1.21218	.00003	10.2279	.01
L β_9	$\beta_9L_{I}M_{V}$	1.20479	.00007	10.2907	.01
L γ_5	$\gamma_5L_{II}N_{I}$	1.13235	.00003	10.949	.1
L_2N_2	$L_{II}N_{II}$	1.1218	.0003	11.052	.01
L_2N_3	$L_{II}N_{III}$	1.1149	.0002	11.12	.01
L γ_1	$\gamma_1L_{II}N_{IV}$	1.09855	.00003	11.2859	10.
L γ_8	$\gamma_8L_{II}O_{I}$	1.08113	.00004	11.4677	.1

Table 3.1. continued

Excitation Line		Wavelength (Angstrom)	Error (Angstrom)	Energy (keV)	Relative Intensity
L_2O_3	$L_{II}O_{III}$	1.0792	.0002	11.488	.01
L V	$V\ L_{II}N_{VI}$	1.0771	.0001	11.51	.01
L γ_6	$\gamma_6 L_{II}O_{IV}$	1.07438	.00005	11.5387	.01
L γ_2	$\gamma_2 L_I N_{II}$	1.06806	.00003	11.608	1.
L γ_3	$\gamma_3 L_I N_{III}$	1.062	.00006	11.6743	2.
L_1N_4	$L_I N_{IV}$	1.0468	.0002	11.844	.01
L γ_{11}	$\gamma_{11} L_I N_V$	1.0458	.0001	11.856	.01
L_1O_1	$L_I O_I$	1.0317	.0003	12.017	.01
L $\gamma_{4,}$'	$\gamma_{4,}{}' L_I O_{II}$	1.02863	.00003	12.053	.1
L γ_4	$\gamma_4 L_I O_{III}$	1.02775	.00003	12.0634	.1
$L_1O_{4,5}$	$L_I O_{IV,V}$	1.025	.0002	12.095	.01
K L_1	K L_I	.21592	.00004	57.42	.01
K α_2	$\alpha_2 K\ L_{II}$	.213828	.000002	57.9817	50.
K $\alpha_{1,2}$	$\alpha_{1,2} K\ L_{II,III}$	.210616	.000006	58.8727	150.
K α_1	$\alpha_1 K\ L_{III}$	.20901	.1E-6	59.3182	100.
K β_3	$\beta_3\ K\ M_{II}$	.185181	.000002	66.9514	12.
K β_1	$\beta_1 K\ M_{III}$	.184374	.000002	67.2443	26.
K $\beta_{5,}$''	$\beta_{5,}{}'' K\ M_{IV}$	.183264	.000005	67.652	.3
K $\beta_{5,}$'	$\beta_{5,}{}' K\ M_V$	.183092	.000007	67.715	.3
K $\beta_{2,}$''	$\beta_{2,}{}'' K\ N_{II}$	.1796	.00001	69.031	10.
K $\beta_{2,}$'	$\beta_{2,}{}' K\ N_{III}$	.179421	.000007	69.101	10.
K β_4	$\beta_4 K\ N_{IV,V}$	.17892	.00002	69.294	.1
K $O_{2,3}$	K $O_{II,III}$	.178444	.000005	69.479	.01

Figure 3.2. Partial x-ray spectrum of the tungsten anode. The number under the wavelengths are the relative intensities of the excitation lines. (Courtesy of Sue-Lein Wang Lii and Dr. R. A. Jacobson)

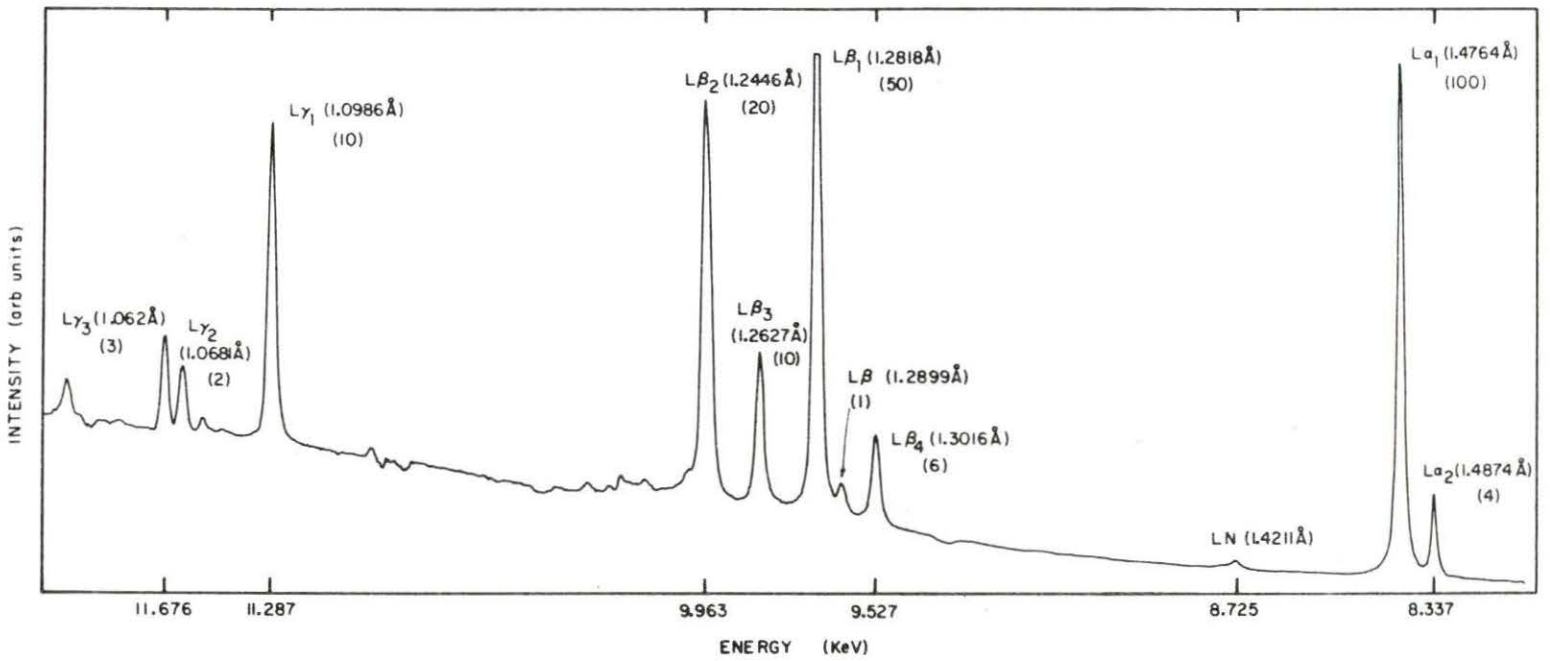
INTENSITY (arb units)
Lγ3 (1.062Å)
(3)
Lγ2
(1.068Å)
(2)
Lγ1 (1.0986Å)
(10)
Lβ2 (1.2446Å)
(20)
Lβ1 (1.2818Å)
(50)
Lβ3
(1.2627Å)
(10)
Lβ (1.2899Å)
(1)
Lβ4 (1.3016Å)
(6)
LN (L4211Å)
La1 (1.4764Å)
(100)
La2 (1.4874Å)
(4)
11.676
11.287
9.963
9.527
8.725
8.337
ENERGY (KeV)

the largest counting rate of the exit beam obtained for each motion. Then the crystals are driven to these new starting positions and the process is repeated until changes in the new starting positions are too small to affect the counting rate of the exit beam. A computer controls the crystal positions through stepping motors. This process and the data collection process is controlled by a BASIC computer program called ROCKPB.

The signal from the lithium-doped silicon, Si(Li), detector is amplified and passed to three single-channel analyzers. This signal contains pulses due to excitation line and harmonic wavelengths which are passed by the monochromator. Since the pulse height (voltage) of the detector is proportional to the energy of the detected photon, the single-channel analyzers will separate the excitation line and various harmonic wavelengths from the signal if the analyzer's voltage windows are set properly. For each scan, three transmitted beam absorption spectra were recorded simultaneously: excitation line, second and third harmonic wavelengths. This method ensures that the wavelengths of the harmonics are as accurate as those of the excitation line.

Seven different high purity crystal wafers were investigated: 2 HOPG, 1 germanium and 4 silicon. The thicknesses of the wafers were measured by an accurate micrometer. The accuracies of the measurements were to $\pm$ 0.0005 cm. The lengths of the crystals were measured by a vernier caliper to an accuracy of $\pm$ 0.05 cm. A summary of these characteristics and crystal sources is in Table 3.2.

Each wafer was mounted on a computer driven goniometer. The

crystal was aligned so that when the plane of the crystal was normal to the beam, the beam path passed through the geometrical center of the crystal. Care was taken to ensure that all rotations of the wafers were done about a vertical axis perpendicular to the beam path (see Figures 3.1 and 1.3). The angular range scanned was from $\phi = 0°$ to 180° with a scan step size of 1.0° or 0.5°. For some crystals, additional scans were taken near the region where the beam is normal to the plane of the crystal (near $\phi = 90°$). The angular range scanned was from $\phi = 85°$ to 95° with a scan step size of 0.05°.

Table 3.2. Dimensional characteristics of the crystals used in this study

Sample	Thickness (cm)	Length (cm)	Source
Ge	0.0194	5.09	Janos Optical Corp.
Si	0.2946	5.08	On loan from Dr. S.A. Werner (Univ. of Missouri at Columbia)
Si	0.0708	5.07	Monsanto
Si	0.0699	5.07	Monsanto
Si	0.0250	5.08	Janos Optical Corp.
HOPG	0.1524	1.2 x 4	Union Carbide-ZYA Grade
HOPG	0.1532	1.5 x 6	Union Carbide-ZYA Grade

Data analysis

All of the scans were analyzed by a FORTRAN computer program called NLS (Nonlinear Least-Squares). The algorithm used is known as the maximum neighborhood method (Marquardt, 1963). It is based on an

interpolation between the Taylor series and gradient methods used to fit nonlinear parameters in a model. Appendix A contains an outline of the development of this method. A subroutine in NLS called CURFIT performs the linearization of the parameters and calculates a new set of parameters using the previously described method. The main routine, NLSFIT, controls the iterations to CURFIT based on goodness of fit calculations of either χ^2 (see Equation A3) or a r-factor. The r-factor is given by (Hamilton, 1964)

$$r = \left[\frac{\sum_i (y_i - f_i)^2 (1/\sigma_i)}{\sum_i (y_i)^2 (1/\sigma_i)} \right]^{1/2} \tag{3.1}$$

where the sums are over all the data, y_i is the i^{th} dependent data point, f_i is the predicted value of the i^{th} dependent data point and σ_i is the uncertainty in the data point y_i. Copies of the major computational subroutines used in NLS are contained in Appendix B. There are modified versions of subroutines published elsewhere (Bevington, 1969). They are:

1. NLSFIT - the main routine which controls the iteration procedure.
2. CURFIT - a subroutine which performs the linearization of the parameters.
3. RCHISQ - a subroutine which calculates the χ^2 and r-factor for weighted and unweighted schemes.
4. DERIVA - a subroutine which non-analytically calculates

derivatives described by Equation A5.

All computations in CURFIT, RCHISQ AND DERIVA are done in double precision where necessary.

The model used in this study is similar to Equation 1.4. The model is

$$I = I_o \exp(- \mu t/\sin (\phi + \varepsilon)) \tag{3.2}$$

where t is the crystal thickness, ϕ the tilt angle of the wafer, ε a phase factor, I_o the incident intensity of the beam and I is the measured transmitted intensity (counting rate). The parameters adjusted by the program are I_o, μ and ε. Variations of the model were also tried such as

$$I = I_{01} \exp(- \mu_1(x + x^2)) + I_{02} \exp(-\mu_2(x + x^2)) \tag{3.3}$$

where $x = t/(\sin(\phi + \varepsilon))$. In most cases, variations of the model did not significantly improve the fit to the data.

Before any type of refinements of the parameters were performed, initial estimates of μ, ε and I_o had to be determined. I_o was determined experimentally by the filter method described in Appendix C. ε could be determined from a plot of I vs ϕ for the raw data. There is a local minimum at $\phi + \varepsilon = 0°$ or $180°$ in these plots. ε may be determined at one of these minima. μ was estimated by interpolating data in the International Tables for X-ray Crystallography (1974). The main routine, NLSFIT, required an operator to adjust these estimates so that

the r-factor was below 0.075. Then the program took control and performed its optimization. Despite the least-squares improvement in the maximum neighborhood method, there are many examples where any least-squares program will converge to an improper minima of χ^2 which is not the principal one. Therefore, manual interactions are necessary to help in finding a local minimum in χ^2 which would have a physical sense.

Additionally, there were several constraints used in fitting the data. Before fitting the model to the data, the data were smoothed with a 3-point smoothing function. Initial estimates for the parameters were entered into the program and all parameters were refined. This was done for each wavelength in a particular scan. Since all three of the intensity patterns are from the same scan, the phase angles, ε, from each fit in the scan were averaged. This average was used in subsequent analysis of the same data. In these cases, ε was not allowed to vary during the calculations of the fitting routine.

CHAPTER 4

Attenuation in Silicon and Germanium

Silicon data results

For the scans collected using the 0.025 cm thick silicon crystal the exit collimator used on the monochromator box was a lead filled, 80 mm brass tube with a round tapered hole 1.0 mm in diameter at the exit end. The counting time set on the counters was 5, 10, and 10 seconds for the fundamental, second and third harmonic wavelengths, respectively. The x-ray source was continuously examined by a monitor (see Figure 3.1). The monitor is a scintillation detector. During the data gathering process, the monitor counting rate was not allowed to fluctuate by more than 5% with respect to the original monitor reference count number set at the beginning of each run.

A representative sample of the scans for the silicon data is given in Figure 4.1. The angular range in the figure is from $\phi = 0°$ to $100°$ with a scan step size of $1.0°$. Since the data are symmetric about $\phi = 90°$ (i.e. when the beam is perpendicular to the plane of the crystal), the rest of the scans for $\phi > 100°$ are not shown. From around $75°$ to $90°$, there seem to be many structure effects (namely multiple reflection effects), some of which may be represented by Bragg dips. To ignore these effects, the data were analyzed excluding the region $80° \leq \phi \leq 100°$. Upon comparing the values of the measured intensities with those of the calculated ones derived from a fit to the model, it was found that the data fit the model very well for all

Figure 4.1. Normalized counting rates versus the tilt angle ϕ for silicon crystal 0.0250 cm thick

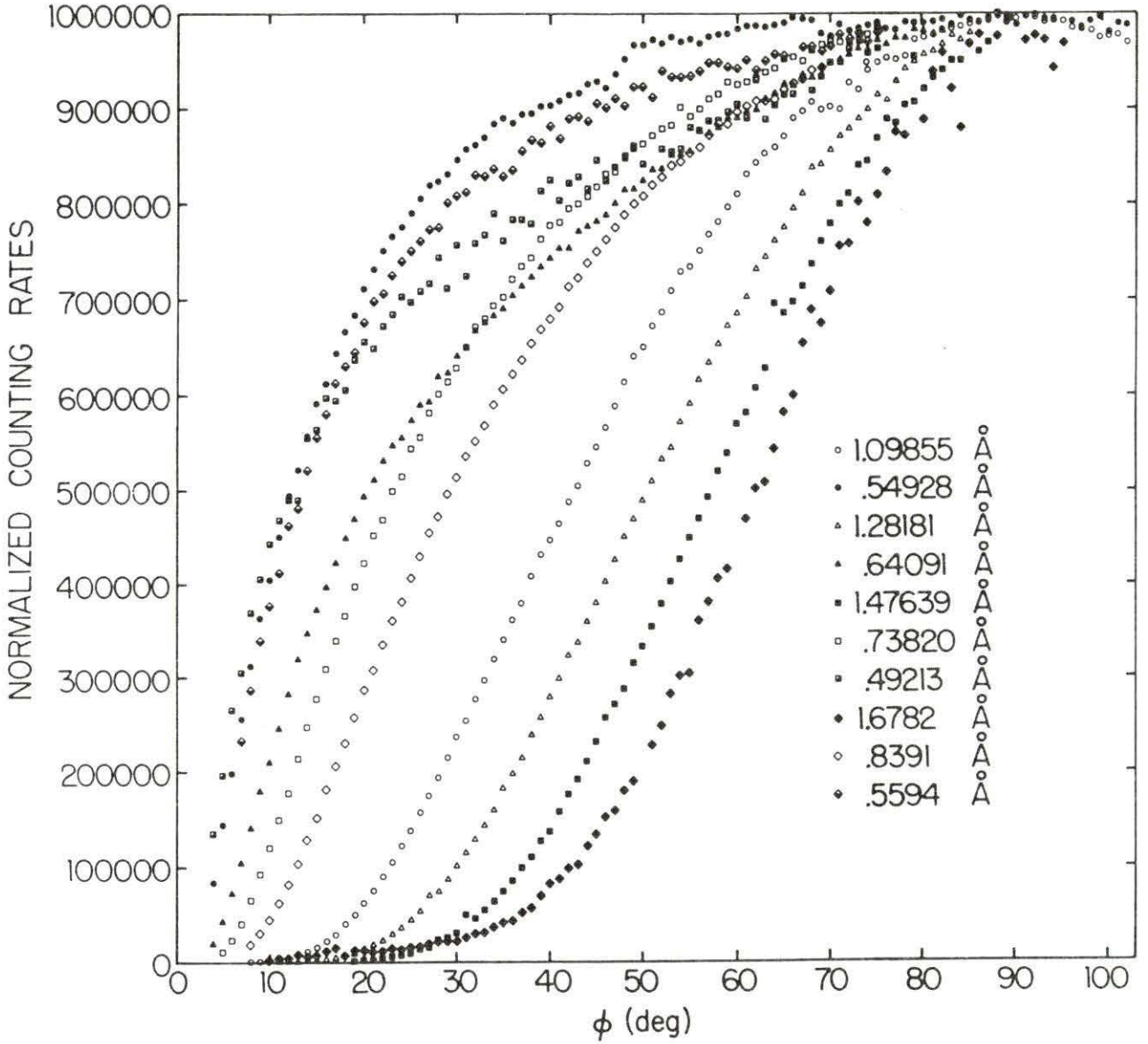
NORMALIZED COUNTING RATES
1000000
900000
800000
700000
600000
500000
400000
300000
200000
100000
0
0
10
20
30
40
50
60
70
80
90
100
ϕ (deg)
1.09855 Å
.54928 Å
1.28181 Å
.64091 Å
1.47639 Å
.73820 Å
.49213 Å
1.6782 Å
.8391 Å
.5594 Å

points except those in the regions where $\phi < 30°$ and $\phi > 150°$. Figure 4.2 shows why this is.

In Figure 4.2, the natural logarithm of the measured intensities for all wavelengths used to study the silicon crystal is plotted against the beam path length divided by the crystal thickness. If the model given by Equation 3.2 is correct, then the plots in Figure 4.2 should be straight lines whose slope is proportional to the attenuation coefficient at that wavelength. In most of the plots, the slopes of the lines are constant in the region $30° \leq \phi \leq 90°$. For $\phi < 30°$, the slopes of the lines change to another constant value for all of the fundamental wavelengths. If Equation 3.2 is valid in this region then the attenuation coefficient has changed. This will be examined later for the case where the wavelength, λ, is 1.28181 Å.

The data for each of the scans were then reanalyzed with the following angular regions excluded from the fit: $\phi < 30°$, $80° \leq \phi \leq 100°$ and $\phi > 150°$. The results of the fitting routine, done by the computer program NLS, on each of the scans are given in Table 4.1. The r-factors and initial intensities calculated by the program are also listed so that the parameters of the model may be compared.

Examination of Equation 3.1 shows that an r-factor of zero implies a perfect fit. That is, the model and its parameters exactly describe the data. For most of the refinements given in Table 4.1, the r-factors are less than 0.01. The notable exceptions are when the wavelength is 1.6782Å, 1.47369Å, 0.42727Å and 0.36618Å. The high r-factor of the two higher wavelengths mentioned may be due to the dips

Figure 4.2. Log(I) versus beam path length divided by the crystal thickness for 0.0250 cm thick silicon crystal. (The up arrows indicate the change of linearity for some of the plots.)

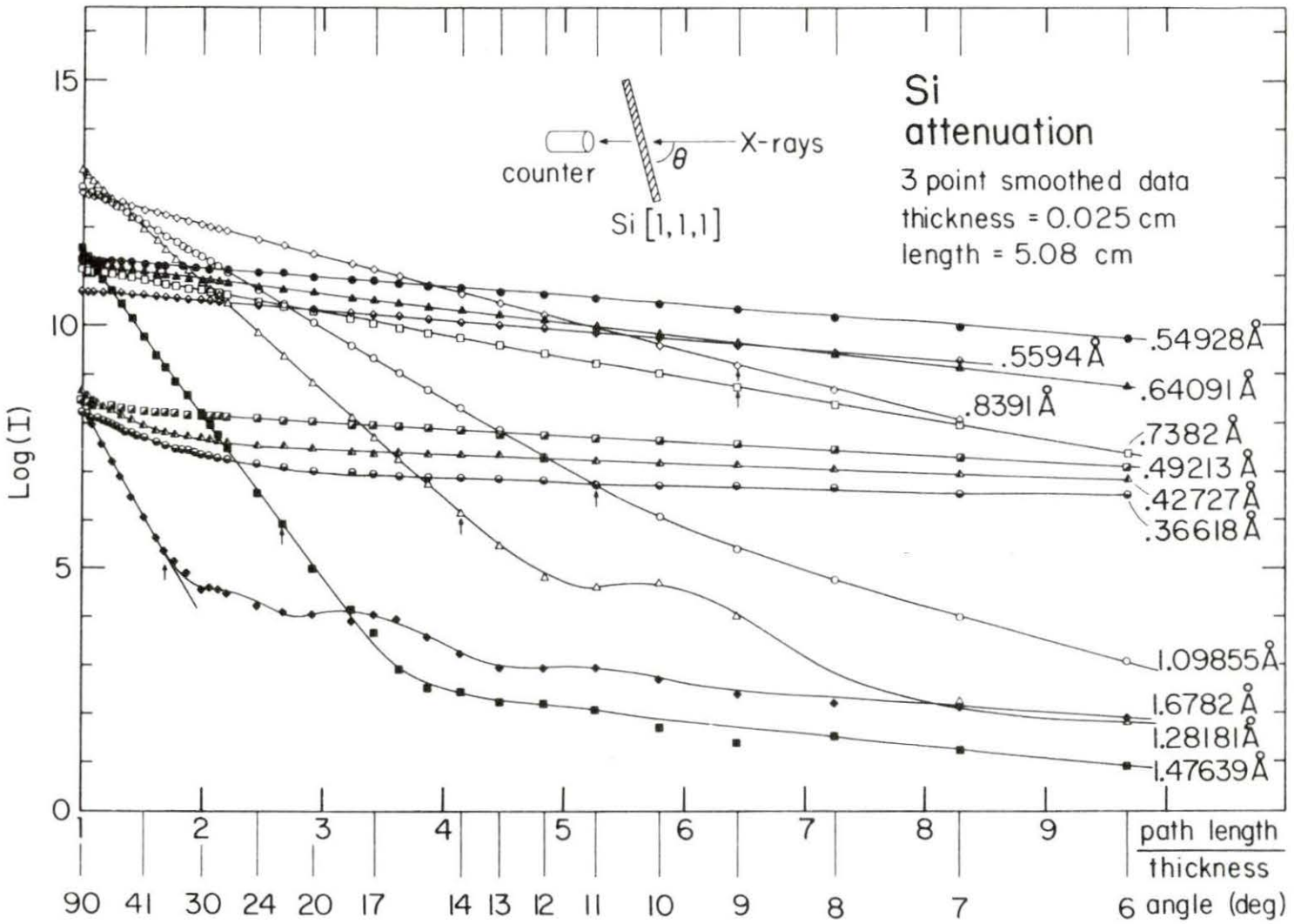
Si
attenuation
3 point smoothed data
thickness = 0.025 cm
length = 5.08 cm
counter
X-rays
θ
Si [1,1,1]
Log (I)
15
10
5
0
.54928Å
.5594 Å
.64091 Å
.8391 Å
.7382 Å
.49213 Å
.42727 Å
.36618 Å
1.09855Å
1.6782 Å
1.28181Å
1.47639Å
1
2
3
4
5
6
7
8
9
path length / thickness
90 41 30 24 20 17 14 13 12 11 10 9 8 7 6 angle (deg)

Table 4.1. Attenuation coefficients for silicon

λ(Å)	$\mu(cm^{-1})$	I_o (counts/c-time)	r-factor($x10^{-2}$)
1.6782	139.2	1700000	1.04
1.47639	194.8	620000	2.07
1.28181	92.20	1700000	0.73
1.09855	57.06	780000	0.96
0.83910	26.27	320000	0.55
0.73820	17.62	100000	0.50
0.64091	11.38	97000	0.87
0.5594	8.108	27000	0.94
0.54927	7.217	100000	0.98
0.49213	5.522	4603	0.98
0.42727	3.922	2400	1.1
0.36618	2.312	1500	1.6

which appear in the data near $\phi = 75°$ (See Figure 4.1). A more important consideration is that the attenuation coefficients for these wavelengths change nearer to $\phi = 30°$ than any other scan as shown in Figure 4.2. The up arrows under some of the plots of Figure 4.2 indicate where the change in linearity takes place. The change in linearity indicates a change in the attenuation coefficient. Since this change in the attenuation coefficient is not accounted for by the model of Equation 3.2, a higher than normal r-factor is expected for any analysis which is performed in a region near this change.

Examination of the initial intensities of Table 4.1 reveals that the higher the order of the harmonic wavelength is, the lower the incident intensity. This is expected since the harmonic wavelengths are

due to higher order Bragg reflections of the monochrometer crystals. The structure factor, F, in Equation 1.2 accounts for the changes in the intensities of the reflected beam due to changes of the order of reflection. Also, the intensity of the reflected beam goes as λ^3. Thus the smaller the wavelength is, the smaller the reflected intensity.

Discussion of the silicon data results

The experimental attenuation coefficients in Table 4.1 are plotted against the wavelength cubed in Figure 4.3. Included in this plot are attenuation coefficients reported by other authors (see Table 4.2) and those which have been calculated from other tabulated data (see Table 4.3). There is very little deviation of all the data from the dashed straight line which is drawn in Figure 4.3. The dashed line is the line of best fit for the attenuation coefficients which were calculated from tabulated data.

These attenuation coefficients were calculated from the total attenuation cross sections, σ, by a method given by the International Tables for X-ray Crystallography (1974). The total attenuation cross sections tabulated therein include photoelectric, coherent and incoherent processes. For a crystal with a unit cell volume, V_c, the linear attenuation coefficient μ, may be calculated by

$$\mu = (1/V_c) \sum_i \sigma_i . \qquad (4.1)$$

The summation is over all atoms in the unit cell. In silicon and germanium crystals, there are 8 atoms per unit cell and the lattice parameters are $a_{Si} = 5.430\text{Å}$ and $a_{Ge} = 5.658\text{Å}$ (Kittel, 1971). For

Figure 4.3. μ versus λ^3 for 0.0250 cm thick silicon crystal. (I.T.C. (4) are linear attenuation coefficients derived from the International Tables for X-ray Crystallography (1974)

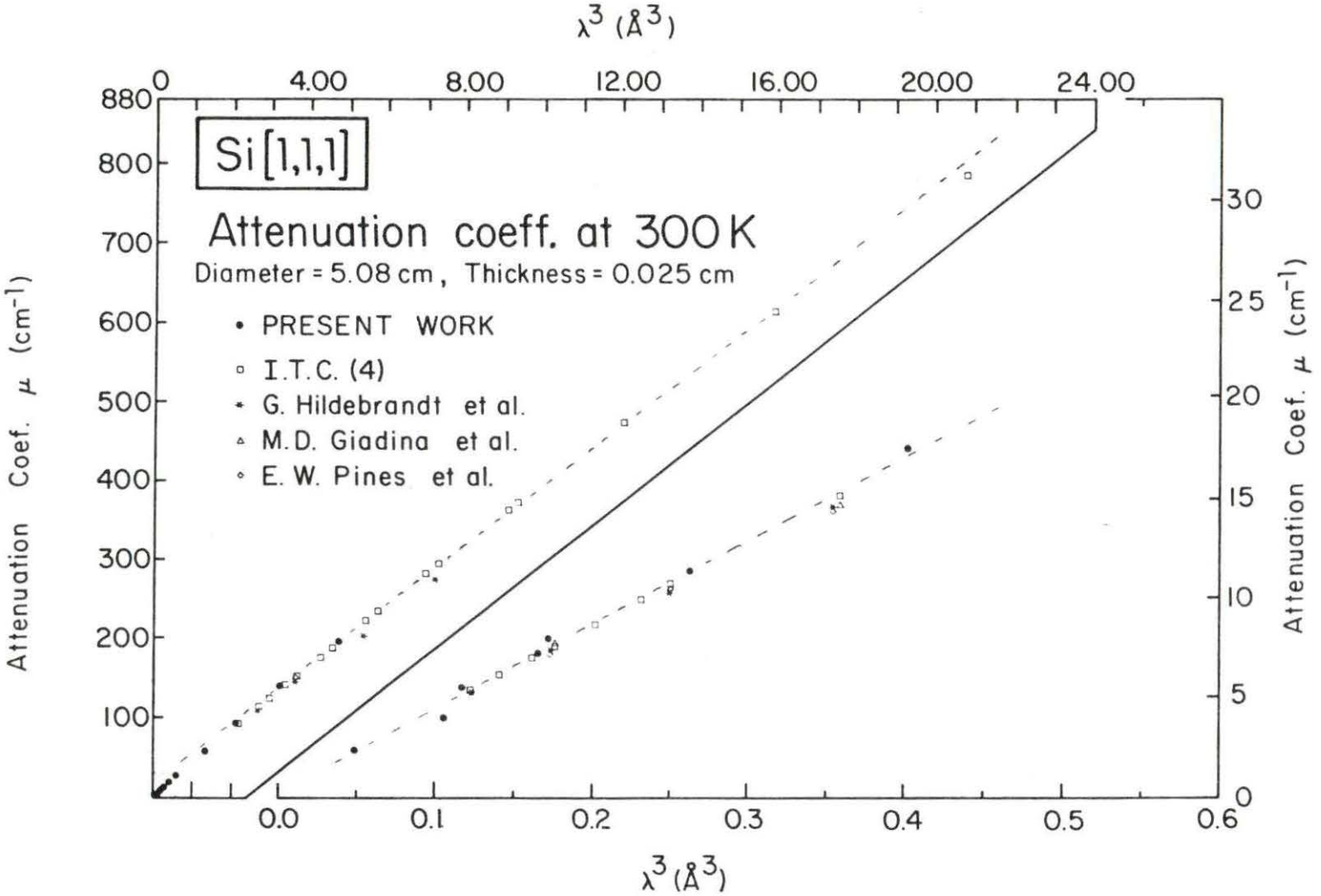
λ³ (Å³)
0
4.00
8.00
12.00
16.00
20.00
24.00
Si [1,1,1]
Attenuation coeff. at 300 K
Diameter = 5.08 cm , Thickness = 0.025 cm
• PRESENT WORK
▫ I.T.C. (4)
* G. Hildebrandt et al.
▵ M.D. Giadina et al.
◇ E. W. Pines et al.
Attenuation Coef. μ (cm⁻¹)
880
800
700
600
500
400
300
200
100
30
25
20
15
10
5
0
0.0
0.1
0.2
0.3
0.4
0.5
0.6
λ³ (Å³)

Table 4.2. Table of total attenuation cross sections, σ with associated linear attenuation coefficients, μ for silicon, germanium and carbon

Target Radiation	λ(Å)	Si		Ge		C	
		σ(barns/atom)[a]	μ(cm^{-1})	σ(barns/atom)[a]	μ(cm^{-1})	σ(barns/atom)[a]	μ(cm^{-1})
Ag Kβ1	0.4970	107.3	5.35	2739	121.0	6.005	0.6829
Pd Kβ1	0.5205	122.4	6.10	3113	137.5	6.363	0.7236
Rh Kβ1	0.5456	140.1	6.98	3547	156.7	6.781	0.7711
Ag Kα	0.5608	151.8	7.57	3830	169.2	7.054	0.8022
Pd Kα	0.5869	173.2	8.63	4345	191.9	7.554	0.8591
Rh Kα	0.6147	198.5	9.89	4943	218.3	8.140	0.9257
Mo Kβ	0.6323	215.7	10.75	5335	235.6	8.546	0.9719
Mo Kα	0.7107	304.7	15.19	7289	321.9	10.67	1.213
Zn Kβ	1.2952	1825	90.97	5097	225.1	49.72	5.654
Cu Kβ	1.3922	2256	112.5	6201	273.9	61.67	7.013
Zn Kα	1.4364	2473	123.3	6750	298.1	67.78	7.708
Ni Kβ	1.5001	2810	140.1	7596	335.5	77.33	8.794
Cu Kα	1.5418	3047	151.9	8186	361.5	84.13	9.567
Co Kβ	1.6208	3519	175.4	9376	414.1	98.02	11.15
Ni Kα	1.6591	3764	187.6	9992	441.3	105.3	11.97
Fe Kβ	1.7565	4434	221.0	11670	515.4	125.6	14.28
Co Kα	1.7902	4684	233.5	12290	542.8	133.3	15.16
Mn Kβ	1.9102	5646	281.4	14670	647.9	163.1	18.55
Fe Kα	1.9373	5878	293.6	15240	673.1	170.4	19.38
Cr Kβ	2.0848	7258	362.6	18630	822.8	214.6	24.40
Mn Kα	2.1031	7439	371.6	19080	842.7	220.6	26.09
Cr Kα	2.2909	9456	472.4	24100	1064.	288.3	32.79
Ti Kβ	2.5138	12260	612.5	31070	1372.	386.0	43.90
Ti Kα	2.7496	15670	782.8	39680	1753.	510.6	58.07

[a]Tabulated in International Tables for X-ray Crystallography (1974).

Table 4.3. Attenuation coefficients measured by other authors for silicon and germanium

Target Radiation	λ(Å)	$\mu_{Ge}(Cm^{-1})$	$\mu_{Si}(C_m^{-1})$
Ag Kβ	0.496	122[a]	5.23[a]
			5.19[b]
Ag Kα	0.558	169[a]	7.32[a]
			7.28[b]
			7.37[c]
Mo Kβ	0.631	236[a]	10.4[a]
			10.4[b]
Mo Kα	0.708	320[a]	14.6[a]
			14.4[b]
			14.6[c]
Cu Kβ	1.389	267[a]	107[a]
Cu Kα	1.538	354[a]	144[a]
			150[b]
Co Kβ	1.617	407[a]	
Fe Kβ	1.753	512[a]	208[a]
Co Kα	1.785	539[a]	
Fe Kα	1.932	681[a]	275[a]
Cr Kβ	2.081	812[a]	
Cr Kα	2.265	1050[a]	

[a]Hildebrandt et al., 1973.

[b]Pike, 1941.

[c]Giardino et al., 1973.

HOPG (carbon), there are 4 atoms per unit cell and the volume of the unit cell is 35.174$\mathring{A}^3$ (Chen et al., 1977). The attenuation coefficients calculated from the above procedure along with the attenuation cross sections are listed in Table 4.2 for silicon, germanium and carbon.

The change in linearity of some of the plots in Figure 4.2 is of great interest. The up arrows under some of the plotted data approximately indicate where the attenuation coefficient changes. To the right of these arrows, the effective attenuation coefficient is much smaller than would otherwise be suspected for the wavelengths indicated.

More scans were made with silicon crystals of different thicknesses to determine if this change in linearity was due to the particular crystal used or if this change is characteristic of the material. The wavelength used for these scans was 1.28181Å. For the two thicker crystals, a longer counting time was used (100 seconds). Also, the scan step size was decreased to 0.4°. The 0.0699 cm thick crystal was scanned in the same manner as the 0.0250 cm one except the scan step size was 0.3°.

The data obtained during the scans are plotted in the form of log (I) versus beam path length in Figure 4.4. There are many interesting features in this plot. When the beam path length is less than 0.2 cm, the slopes of the plots are the same for the 0.0250, 0.0699, and 0.1407 cm thick crystals. The 0.1407 cm thick crystal was actually two crystal wafers put back to back and mounted in the diffractometer.

Figure 4.4. Log(I) versus beam path length for various silicon crystals. (All of the plots start at $\phi = 90°$. $\lambda = 1.28181\text{Å}$ for all scans.)

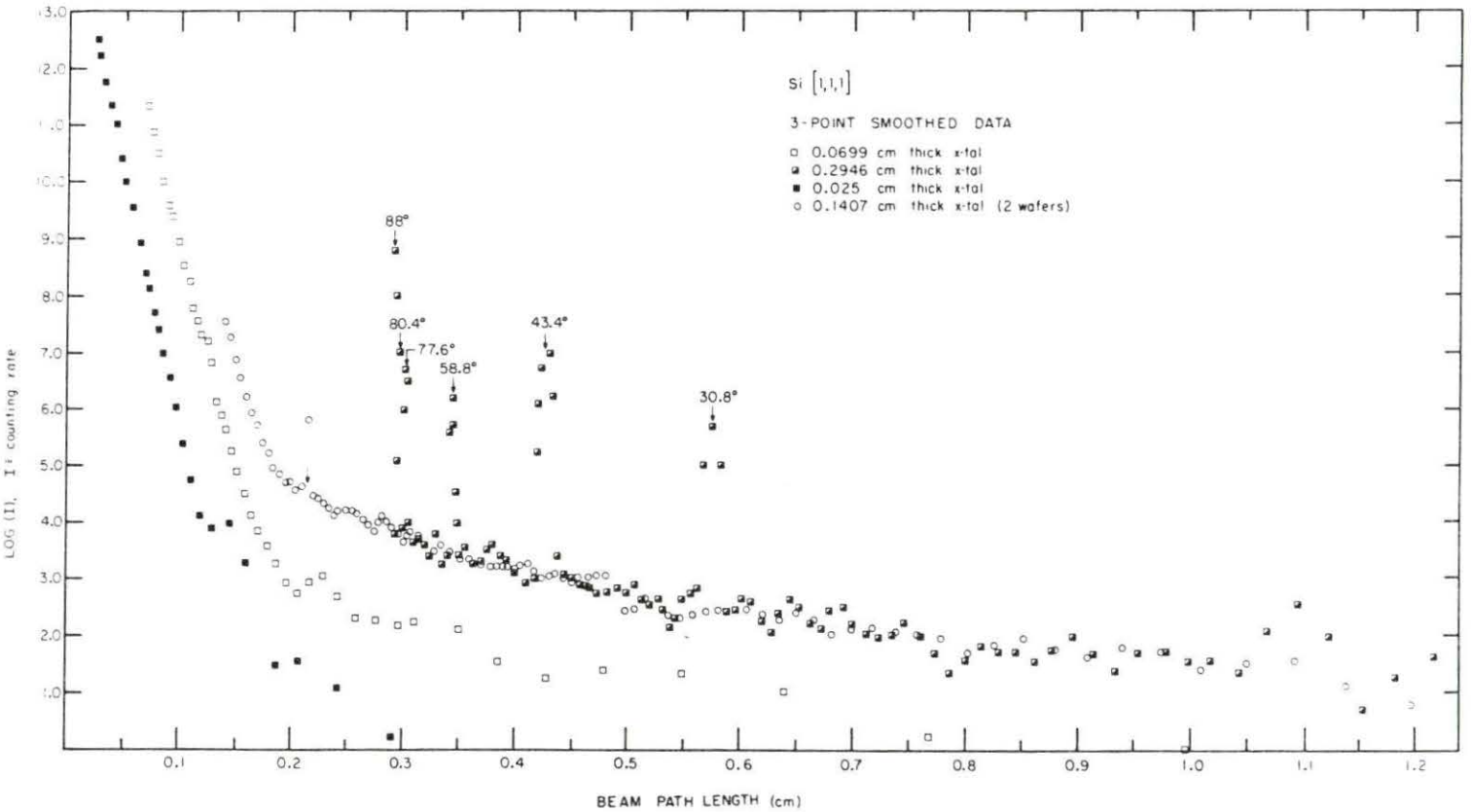
Si [1,1,1]
3-POINT SMOOTHED DATA
0.0699 cm thick x-tal
0.2946 cm thick x-tal
0.025 cm thick x-tal
0.1407 cm thick x-tal (2 wafers)
88°
80.4°
77.6°
58.8°
43.4°
30.8°
LOG (I), I° counting rate
BEAM PATH LENGTH (cm)

To the right of 0.2 cm the linearity changes so that the slope is different. For all of the plots, the effective attenuation coefficient changes after the beam path length through the crystal is greater than 0.2 cm. In the plot of the data for the 0.2946 cm thick crystal are peaks which are due to the Borrmann effect: anomalous transmission. The angles given for the centroids of the peaks are approximate since most of the peaks had only a few points. The mechanism responsible for the anomalously transmitted peak is explained by the dynamical theory of x-rays. When $\mu t > 10$, a standing wave due to multiple reflections is set up within the crystal. At the Bragg condition, the nodes of the standing wave are at the atomic planes and very little of the wave is attenuated through photoelectric attenuation. When this occurs, much of the beam is transmitted. (Much has been written about the dynamical theory of x-ray diffraction. See, for example, Pinsker, 1978; Batterman and Cole, 1964; James, 1982.) In the plot of data for the 0.1407 cm thick crystal there are no peaks present. Since this specimen is actually two crystals and cannot be considered a perfect one, no anomalous transmission peaks are expected.

An attempt was made to analyze the data obtained from the 0.1407 cm thick crystal. Only data in the region where the beam path length was greater than 0.25 cm were considered. The data were smoothed with a three point smoothing function and then analyzed with the computer program NLS described in Chapter 3. It was found that the attenuation coefficient in this region is 3.1 cm^{-1}. The fit of the model to the data was extremely poor with an r-factor of 0.096. The poor fit is due in part to low counting rates.

Analysis of the second and third harmonics of the $L\beta_1$ line (λ = 1.28181Å) are not given. The results of the plot of Log (I) versus beam path length for this data indicate that the attenuation coefficient does not change as a function of the crystal thickness.

Silicon data conclusions

For the thin silicon crystals where the effective thickness is less than 0.05 cm, it has been found that this technique for determining the attenuation coefficient is accurate in terms of model fitting. Comparison of these attenuation coefficients with those which have been published elsewhere, reveals that the attenuation coefficients have the same wavelength dependency. That is, the attenuation coefficients are proportional to the wavelength cubed (see Figure 4.3).

When the intensity patterns for the thicker silicon crystals have been measured, plots of log (I) versus beam path length show that the linear attenuation coefficient changes. For the perfect thick crystal (t = 0.2946 cm), these plots revealed the presence of anomalous transmission peaks (see Figure 4.4). These peaks can be explained by dynamical effects and normally appear when $\mu t > 10$. Here t is the beam path length and μ is the linear attenuation coefficient. Examination of Figure 4.4 shows that the change in linearity of the plotted data occurs when t = 0.2 cm. In this case, $\mu = 92.20\ cm^{-1}$ and $\mu t = (92.2\ cm^{-1})(0.2\ cm) = 18.4$. From this, one might conclude that the changes in linearity of the plots in Figures 4.2 and 4.4 are entirely due to dynamical effects. This, however, may not be true since the change in linearity also occurs for the somewhat imperfect crystal

(t = 0.1407 cm) which was made by placing two crystal wafers back to back.

Germanium data results

The experimental conditions for the germanium data aquisition were the same as those for the silicon. Due to low counting rates, for some of the scans, the times on the pulse counters were set at 60, 60 and 60 seconds for the fundamental, second and third harmonic wavelengths, respectively. Additionally, a measurement was taken using the fourth harmonic wavelength of the tungsten L1 excitation line (λ = 0.4196Å).

The analysis of the data for all the germanium scans was done in the range $30° \leq \phi \leq 80°$. Examination of Figure 4.5 reveals a change in linearity in the plots of log (I) versus beam path length. The model used to analyze the data (Equation 3.2) is valid only where these plots are linear. The angular range was chosen for convenience in the linear region of the plots in Figure 4.5. The results of the analysis for all of the wavelengths studied are listed in Table 4.4.

Compared to the silicon results the r-factors in Table 4.3 are significantly higher in all cases. This may be attributed to structure effects which are not accounted for in the model. In the case of the longer wavelengths, there is the additional problem of x-ray fluorescence due to the proximity of the K-absorption edge.

Discussion of germanium data results

In Figure 4.6, the attenuation coefficients for germanium are plotted against the wavelength cubed. The attenuation coefficients calculated from the International Tables for X-ray Crystallography (1974) are listed in Table 4.2. Attenuation coefficients measured by Hildebrandt are listed in Table 4.3. The dashed line in Figure 4.5 is the line of

Figure 4.5. Log(I) versus beam path length for the germanium crystal. (The data have been normalized and all plots start at $\phi = 90°$ when viewed from left to right)

Ge

THICKNESS – 0.0194 CM

DIAMETER – 5.09 CM

TEMPERATURE – 300 K

3-POINT SMOOTHED DATA

COUNT #'s NORMALIZED

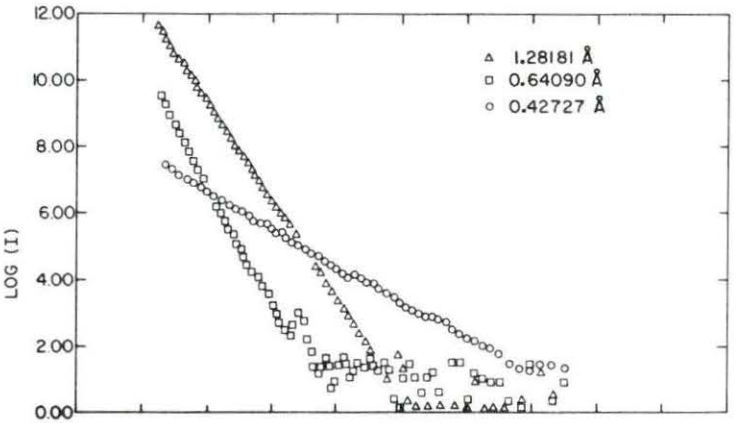

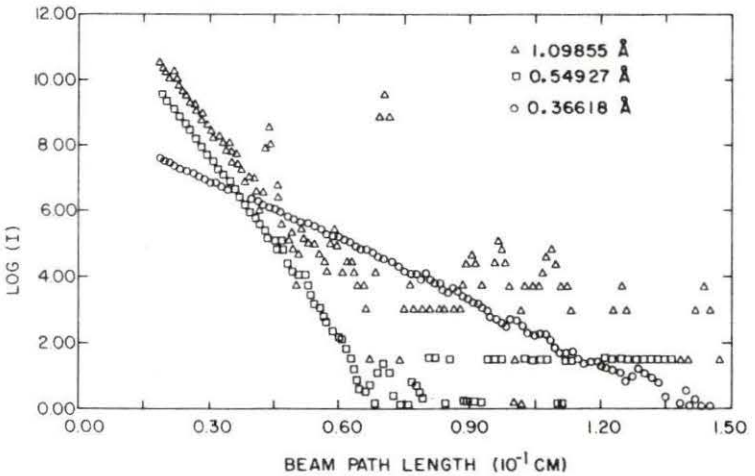

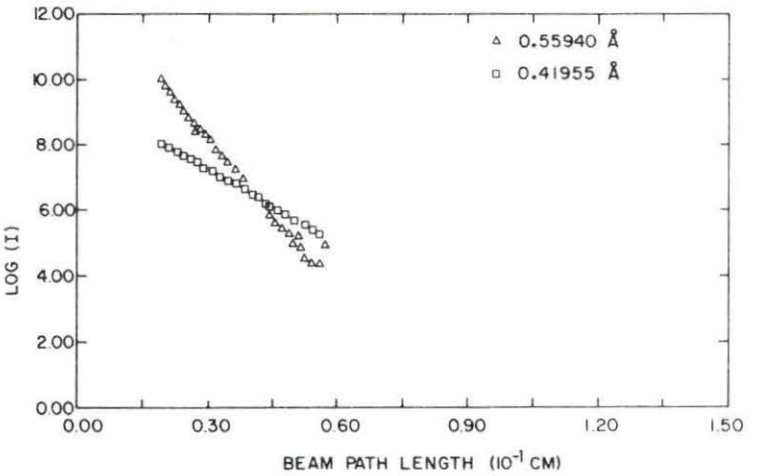

Figure 4.6. μ versus λ^3 for the gernamium crystal. (I.T.C. (4) are data calculated from the International Tables for X-ray Crystallography (1974))

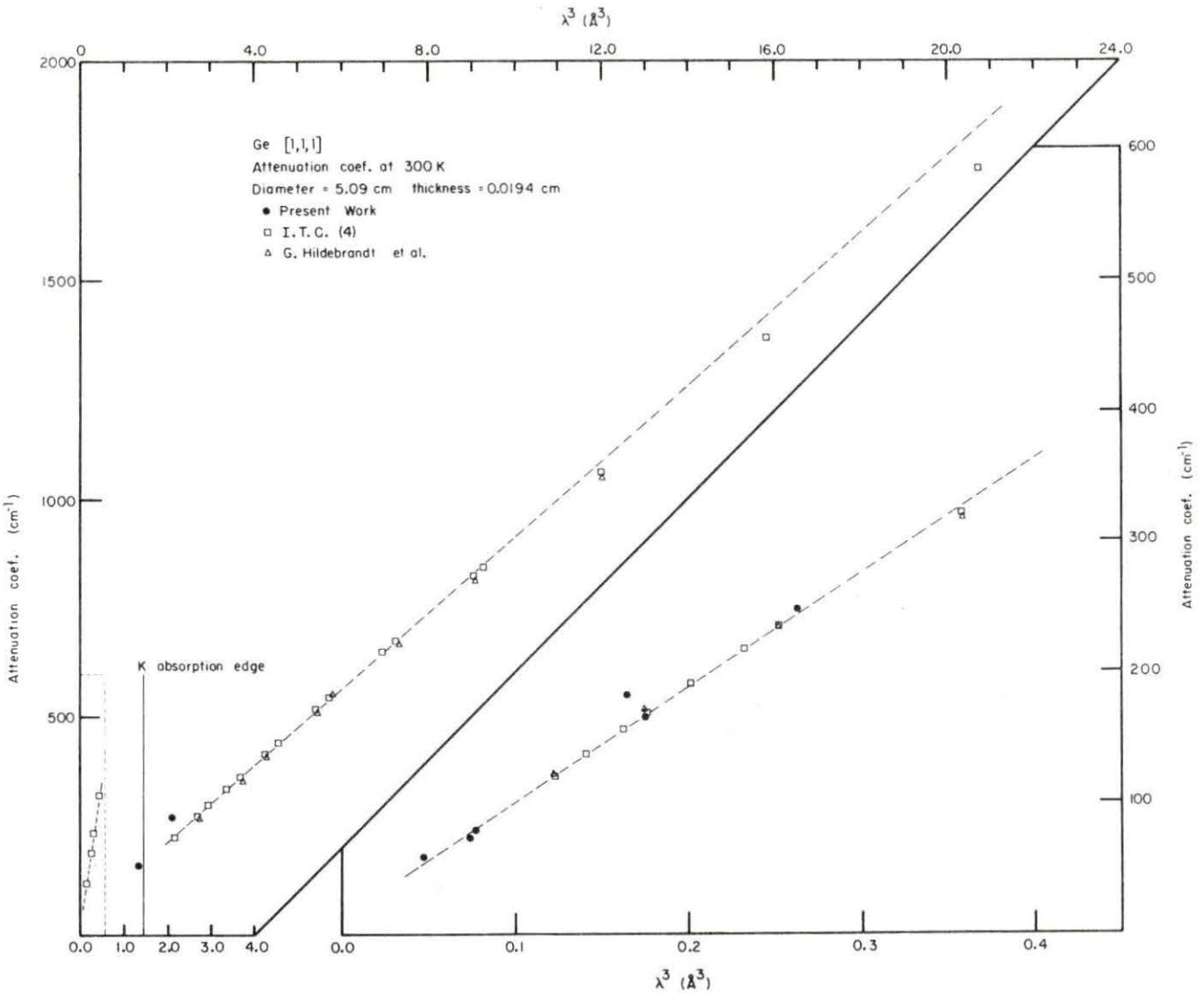
λ³ (Å³)
0
4.0
8.0
12.0
16.0
20.0
24.0
2000
1500
1000
500
Ge [1,1,1]
Attenuation coef. at 300 K
Diameter = 5.09 cm thickness = 0.0194 cm
● Present Work
□ I.T.C. (4)
△ G. Hildebrandt et al.
K absorption edge
Attenuation coef. (cm⁻¹)
600
500
400
300
200
100
0.0
1.0
2.0
3.0
4.0
0.0
0.1
0.2
0.3
0.4
λ³ (Å³)

Table 4.4. Attenuation coefficients for germanium

λ(Å)	$\mu(cm^{-1})$	I_o(counts/c-time)	r-factor(10^{-2})
1.28181	277.0	4.4×10^9	5.3
1.09855	157.3	7.9×10^5	6.2
0.64091	197.3	5.1×10^6	2.7
0.5594	168.1	1.7×10^5	1.2
0.54927	182.15	8.7×10^5	0.73
0.42727	79.54	7.3×10^5	2.5
0.4196	72.87	8.3×10^3	2.2
0.36618	58.40	9.3×10^3	1.13

One interesting feature of the plot in Figure 4.5 is the discontinuity at $\lambda^3 = 1.404 Å^3$. This discontinuity is due to the K absorption edge of germanium at $\lambda = 1.12Å$ and it is a consequence of Equation 2.12. If $\mu = C\lambda^n$ for wavelengths below the K absorption edge, then only the form is valid above the K absorption edge but the constants C and n are different.

Another interesting feature of this plot is that the attenuation coefficients do not seem to follow a linear behavior as a function of λ^3. This is not inconsistent with what has been stated previously in Chapter 2. The exponent does not have to be 3 but only near 3. In fact, Grimvall and Persson (1969) have measured attenuation coefficients of germanium for wavelengths greater than 1.12Å and have calculated an exponent of 2.85 from their data.

The peaks in Figure 4.6 are due to anomalous transmission of x-rays in the germanium. They appear in the longer wavelength plots because the attenuation coefficients are larger at these wavelengths. The condition, $\mu t > 10$, is achieved sooner in terms of beam path length through the crystal and anomalous transmission peaks may be observed.

Germanium data conclusions

From the results plotted in Figure 4.6, most of the measured attenuation coefficients seem to lie close to the dashed line explained earlier. The most notable exception to this are at $\lambda^3 = 2.1\text{Å}^3$ ($\lambda = 1.28181\text{Å}$) and $\lambda^3 = 1.3\text{Å}^3$ ($\lambda = 1.09855\text{Å}$). The reason for this behavior is due to the fact that these wavelengths are just above and below the germanium K absorption wavelength ($\lambda = 1.12\text{Å}$).

The plots of log (I) versus beam path length show a change in attenuation coefficient for the longer wavelengths. This is similar to the results obtained for the silicon measurements. In general, the attenuation coefficients seem to change to a smaller value for a given wavelength when the effective crystal thickness increases beyond a certain point.

CHAPTER 5

Attenuation in HOPG

HOPG data results

The experimental conditions for measuring the transmitted x-ray intensities through HOPG are the same as those described for the thin silicon crystal (t = 0.0250 cm) in Chapter 4. Calculations by NLS, for obtaining the attenuation coefficients of HOPG, were done for both crystals (see Table 3.2) as per the procedure given in Chapter 3. Only attenuation coefficients at the temperature T = 300K were determined for the 0.1532 cm thick crystal. Results of the fitting routine, NLS, for this crystal are reported in Table 5.1. The r-factors seem to be high for the fits where the wavelength is 0.73820Å, 0.64091Å, and 0.54927Å. This is due in part to large fluctuations of the data around the model.

Attenuation coefficients at the temperature T = 300, 200, 150, 100, 50, 15, and 7.0K were determined for the 0.1532 cm thick crystal. This temperature range was achieved by using a He gas, closed 2-cycle refrigeration unit. The refrigerator head was mounted on the goniometer with the 0.1532 cm thick crystal mounted inside. One beryllium vacuum shroud (0.25 mm wall thickness) and two beryllium radiation shields (0.1 mm wall thickness) isolated the crystal from the outside while allowing the x-ray beam to pass through. Measurements were done by first fixing the monochrometer wavelengths: excitation line, second and third harmonics. While keeping these wavelengths fixed, the temperature was

Table 5.1. Attenuation coefficients for HOPG

$\lambda(\mathring{A})$	$\mu(cm^{-1})$	I_o(counts/c-time)	r-factor ($x10^{-2}$)
1.6782	12.51	2.2×10^5	2.32
1.47639	7.990	4.6×10^5	2.82
1.28181	5.584	6.7×10^5	0.78
1.09855	3.659	1.7×10^5	0.76
0.83910	1.692	3.0×10^4	0.85
0.73820	1.471	5.5×10^3	6.10
0.64091	1.323	7.2×10^3	3.71
0.5594	0.8332	6.7×10^3	0.97
0.54927	1.223	3.9×10^4	4.00

changed for each scan. The power of the x-ray source was kept constant between changes of the monochrometer wavelengths. An additional constraint in fitting the model to the data was used based on the above.

The phase angle was refined by using a procedure similar to the one described in Chapter 3. After the phase angle was determined, only data in the range of $100° \leq \phi \leq 150°$ were used for refining the remaining parameters. The incident intensity, I_o, of each wavelength should be constant for all temperature since the wavelengths and x-ray source power were fixed.

Figure 5.1. Normalized counting rate versus ϕ near 90° for the 0.1532 cm thick HOPG crystal

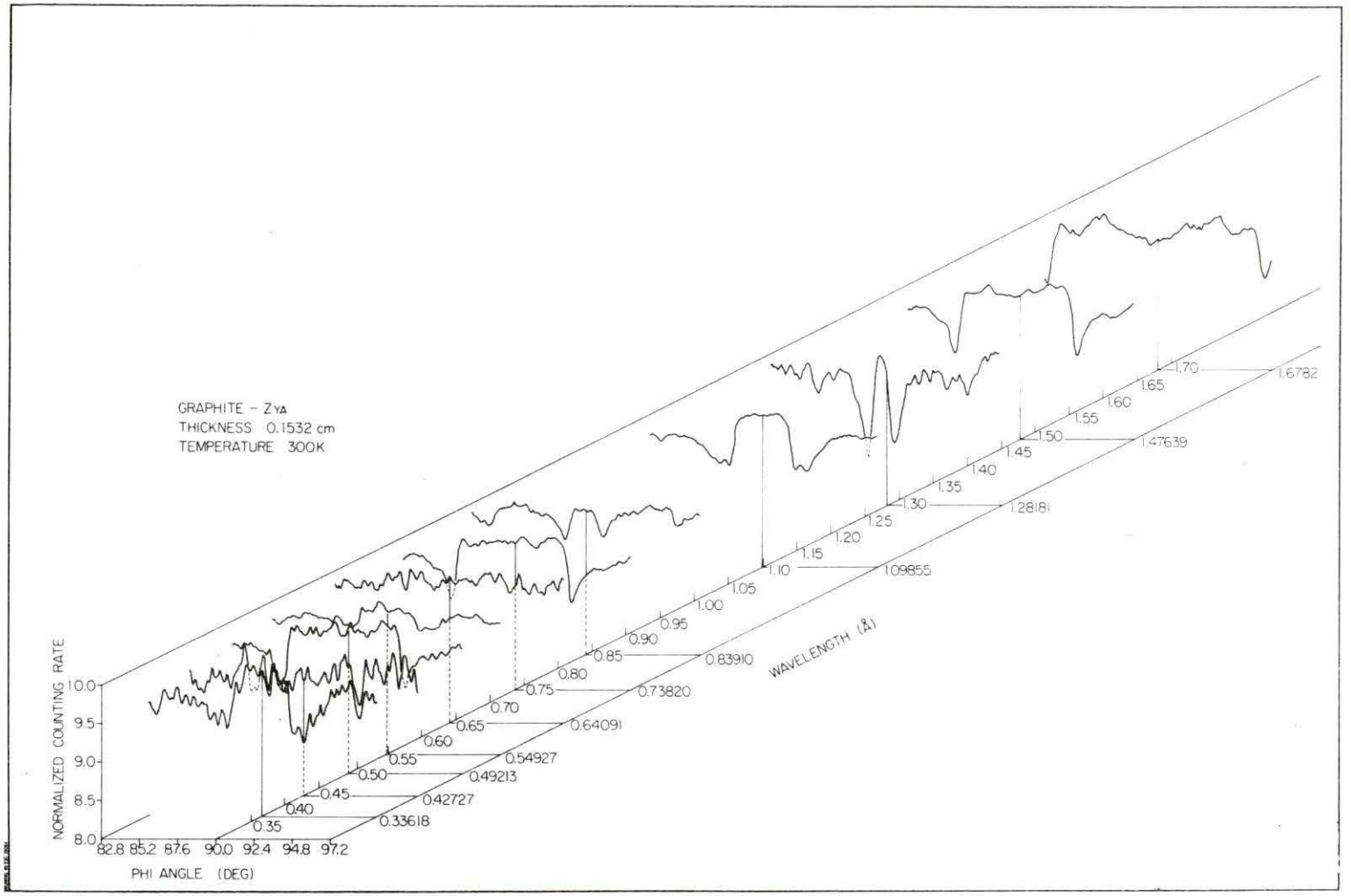
GRAPHITE - ZYA
THICKNESS 0.1532 cm
TEMPERATURE 300K
NORMALIZED COUNTING RATE
10.0
9.5
9.0
8.5
8.0
82.8 85.2 87.6 90.0 92.4 94.8 97.2
PHI ANGLE (DEG)
0.35
0.40
0.45
0.50
0.55
0.60
0.65
0.70
0.75
0.80
0.85
0.90
0.95
1.00
1.05
1.10
1.15
1.20
1.25
1.30
1.35
1.40
1.45
1.50
1.55
1.60
1.65
1.70
0.33618
0.42727
0.49213
0.54927
0.64091
0.73820
0.83910
1.09855
1.28181
1.47639
1.6782
WAVELENGTH (Å)

The procedure for performing a fit on the data for the 0.1532 cm thick crystal is:

1. Do a preliminary fit of all the parameters of the model on the complete data for the excitation line and harmonic wavelengths using NLS.

2. Do Step 1 for all temperature using the same excitation line and harmonic wavelengths.

3. Average the phase angles for all the preliminary refinements in Step 2. Use this average in subsequent refinements. Do not refine the phase angle again.

4. Apply the angular constraint, $100° \leq \phi \leq 150°$, to the data used in the refinement. Use NLS to determine I_o of each wavelength in a scan.

5. Do Step 4 for all temperatures using the same set of wavelengths.

6. Average I_o over the temperatures used. Do this for each wavelength.

7. Refine the last parameter, μ, for all wavelengths and all temperatures using the fixed value of the averaged I_o determined for each wavelength.

The range of data used in the fitting routine was determined in exactly the same manner as that for the silicon data. Plots of normalized counting rates versus ϕ for the wavelengths used to study HOPG are presented in Figure 5.1. These plots are obtained from separate scans done after each scan used to calculate attenuation coefficients. The

Figure 5.2. Log(I) versus beam path length for 0.1532 cm thick HOPG crystal. (As viewed from left to right, all plots start at $\phi = 90°$)

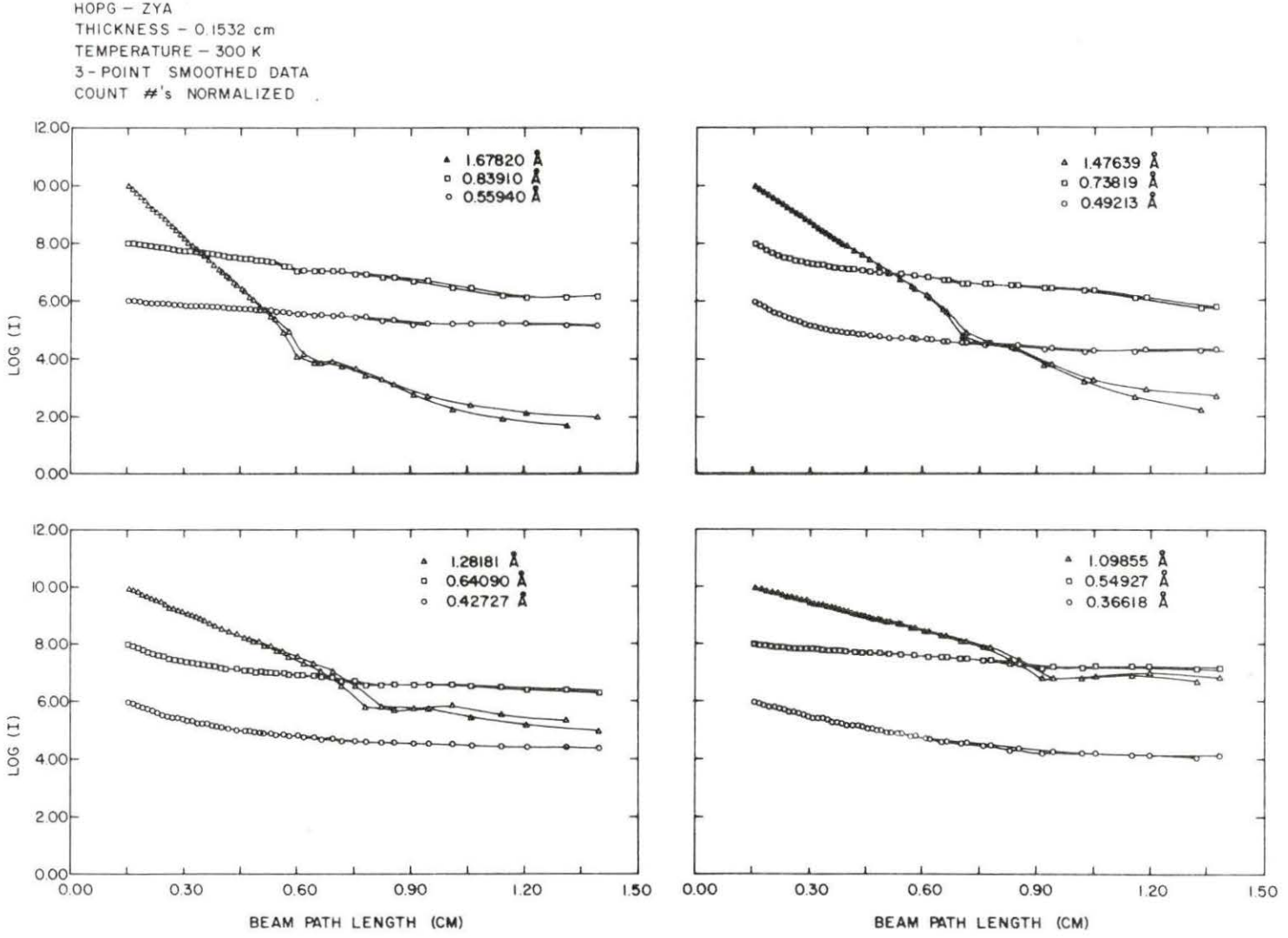
HOPG – ZYA
THICKNESS – 0.1532 cm
TEMPERATURE – 300 K
3-POINT SMOOTHED DATA
COUNT #'s NORMALIZED
1.67820 Å
0.83910 Å
0.55940 Å
1.47639 Å
0.73819 Å
0.49213 Å
1.28181 Å
0.64090 Å
0.42727 Å
1.09855 Å
0.54927 Å
0.36618 Å
LOG (I)
BEAM PATH LENGTH (CM)
0.00
0.30
0.60
0.90
1.20
1.50
2.00
4.00
6.00
8.00
10.00
12.00

scan step size for these scans near $\phi = 90°$ was 0.05°. These plots show the difficulty of measuring attenuation of x-rays near the normal to the crystal ($\phi = 90°$) since there are so many dips present.

In Figure 5.2, log (I) is plotted against the beam path length for all of the wavelengths used to study the 0.1532 cm thick crystal at 300K. If the model (Equation 3.2) is correct then these plots must be straight lines. Each plot, from left to right, starts out linear with a negative slope. Then each plot begins to curve so that the slopes of all the plots seem to approach the same value. From these plots, it was deduced that the most linear regions are those when the data are in the angular range of $90° \leq \phi \leq 150°$.

The results of the attenuation coefficients for various x-ray wavelengths and temperature in HOPG are given in Tables 5.2 through 5.8. As stated earlier in Chapter 2, the attenuation coefficients are proportional to the wavelength cubed. This implies the smaller the wavelength becomes, the smaller the attenuation coefficient. This is true in most reported attenuation coefficients in Tables 5.2 through 5.8. The notable exceptions to this trend are attenuation coefficients calculated for the following wavelengths: 0.73820Å, 0.64091Å, 0.49213Å, 0.42727Å, and 0.36618Å. In each case , the attenuation coefficients seem entirely too large.

Discussion of HOPG results

In Figure 5.1 are scans of the raw data near $\phi = 90°$. These plots show the difficulty of experimentally determining the attenuation coefficients. This figure contradicts statements made by other authors

Table 5.2. Attenuation coefficients for HOPG, T = 300K

λ(Å)	$\mu(cm^{-1})$	I_o(counts/c-time)	r-factor ($x10^{-2}$)
1.6782	12.23	2.2×10^5	1.2
1.47639	8.706	6.3×10^5	1.7
1.28181	5.737	9.6×10^5	0.89
1.09855	3.321	4.6×10^5	2.9
0.83910	1.720	7.8×10^4	0.40
0.73820	5.785	1.0×10^5	0.90
0.64091	5.171	2.4×10^5	0.68
0.5594	1.033	9.6×10^3	1.8
0.54927	1.270	6.8×10^4	0.49
0.49213	5.400	1.7×10^4	6.1
0.42727	5.216	1.6×10^4	0.87
0.36618	2.942	5.5×10^3	2.4

Table 5.3. Attenuation coefficients for HOPG, T = 200K

λ(Å)	$\mu(cm^{-1})$	I_o(counts/c-time)	r-factor ($x10^{-2}$)
1.6782	12.23	2.2×10^5	1.0
1.47639	8.563	6.3×10^5	1.5
1.28181	5.712	9.6×10^5	0.82
0.83910	1.730	7.8×10^4	0.43
0.73820	5.696	1.0×10^5	0.92
0.64091	5.150	2.0×10^5	0.60
0.5594	1.030	9.6×10^3	2.50
0.49213	5.410	1.7×10^4	5.6
0.42727	5.146	1.6×10^5	0.85

Table 5.4. Attenuation coefficients for HOPG, T = 150K

$\lambda(\mathring{A})$	$\mu(cm^{-1})$	I_o(counts/c-time)	r-factor($x10^{-2}$)
1.6782	12.15	2.2×10^5	1.3
1.28181	5.712	9.6×10^5	0.83
1.09855	3.462	4.6×10^5	0.78
0.83910	1.718	7.8×10^4	0.59
0.64091	4.970	2.0×10^5	2.3
0.5594	1.039	9.6×10^3	1.7
0.54927	1.142	6.8×10^4	0.37
0.42727	5.148	1.6×10^4	0.68
0.36618	2.957	5.5×10^3	1.6

Table 5.5. Attenuation coefficients for HOPG, T = 100K

$\lambda(\mathring{A})$	$\mu(cm^{-1})$	I_o(counts/c-time)	r-factor($x10^{-2}$)
1.47639	8.290	6.3×10^5	1.8
1.28181	5.612	9.6×10^5	0.90
0.73820	5.473	1.0×10^5	0.80
0.64091	4.960	2.0×10^5	1.7
0.49213	5.198	1.7×10^4	5.6
0.42727	5.069	1.6×10^5	0.8

Table 5.6. Attenuation coefficients for HOPG, T = 50K

λ(Å)	$\mu(cm^{-1})$	I_o(counts/c-time)	r-factor($x10^{-2}$)
1.09855	3.330	4.6×10^5	3.0
0.54927	1.249	6.8×10^4	0.42
0.36618	3.01	5.5×10^3	1.7

Table 5.7. Attenuation coefficients for HOPG, T = 15.0K

λ(Å)	$\mu(cm^{-1})$	I_o(counts/c-time)	r-factor($x10^{-2}$)
1.6782	11.52	2.2×10^5	1.3
1.47639	8.052	1.5×10^6	1.3
0.83910	1.408	7.8×10^4	0.6
0.73820	6.052	2.2×10^6	1.1
0.5594	0.4979	9.6×10^3	5.4
0.49213	5.143	3.4×10^4	5.6

Table 5.8. Attenuation coefficients for HOPG, T = 7.0K

λ(Å)	$\mu(cm^{-1})$	I_o(counts/c-time)	r-factor($x10^{-2}$)
1.28181	5.491	9.5×10^5	0.91
1.09855	3.420	4.6×10^5	0.93
0.64091	4.911	2.4×10^5	0.54
0.54927	1.171	6.8×10^4	0.49
0.42727	4.936	1.6×10^4	0.82
0.36618	2.994	5.5×10^3	1.40

Figure 5.3. μ versus λ^3 for HOPG crystals at T = 300K. (I.T.C. (4) are data calculated from the International Tables for X-ray Crystallography (1974))

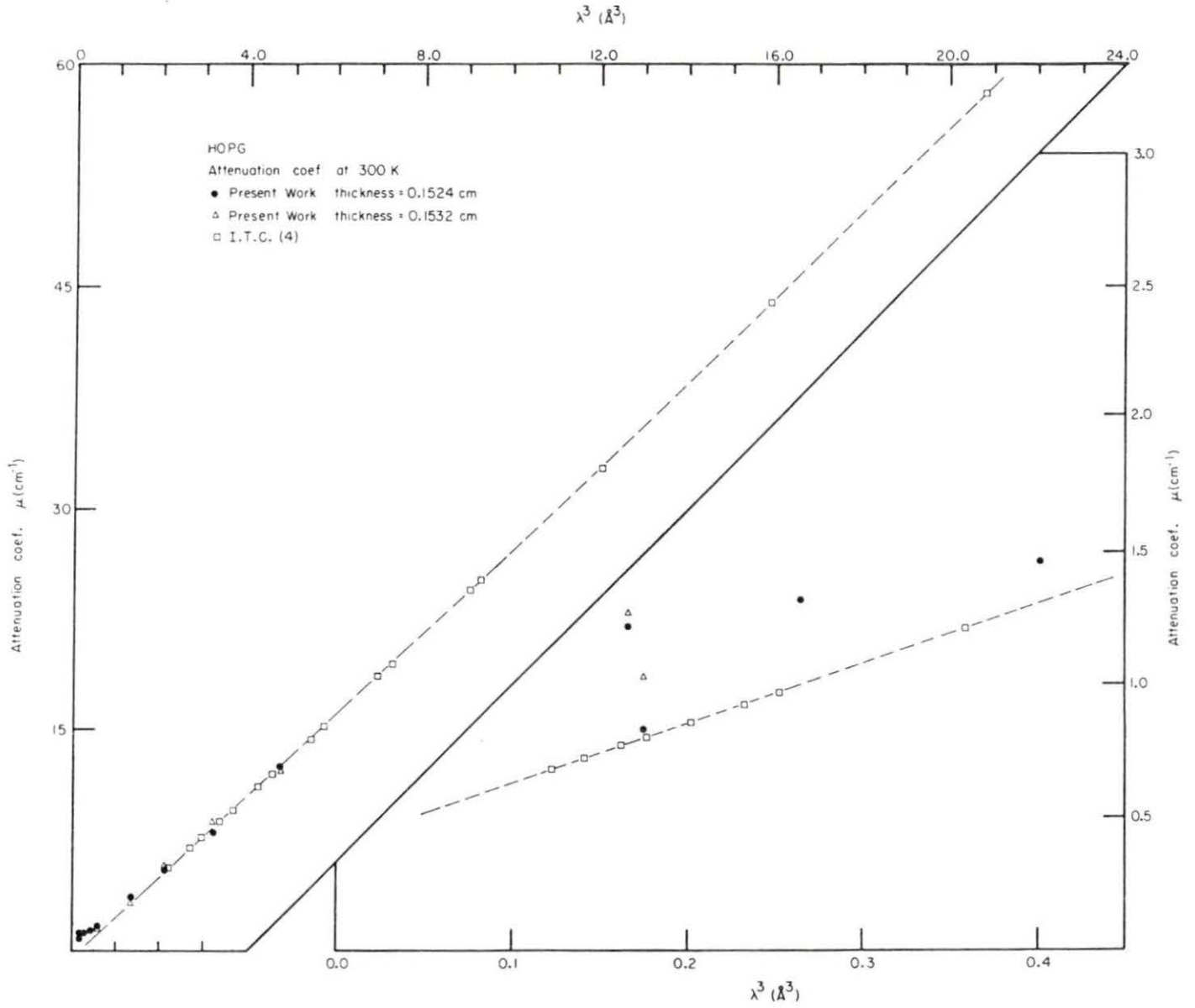
λ³ (Å³)
0
4.0
8.0
12.0
16.0
20.0
24.0
60
45
30
15
HOPG
Attenuation coef at 300 K
● Present Work thickness = 0.1524 cm
△ Present Work thickness = 0.1532 cm
□ I.T.C. (4)
Attenuation coef. μ(cm⁻¹)
3.0
2.5
2.0
1.5
1.0
0.5
0.0
0.1
0.2
0.3
0.4
λ³ (Å³)

(Calvert et al., 1976). They state, "...for pyrolytic graphite and Cu Kα, radiation [λ = 1.54Å], a region of zero excitation is found to exist near ω = 90°. In fact, a plateau extends from ω = 87° to 93°." While in the present study, Cu $K\alpha_1$ radiation was not used, the wavelengths near 1.54Å clearly show a slight dip in intensity near φ = 90°.

The computed attenuation coefficients in Tables 5.1 and 5.2 are plotted against the wavelength cubed in Figure 5.3. Included in this plot are attenuation coefficients reported in Chapter 4 for carbon (see Table 4.2). For the larger wavelengths, there is very little deviation of the experimental data from the straight line drawn in Figure 5.3. The dashed line is the line of best fit derived from the calculated attenuation coefficients for carbon in Table 4.2. For the smaller wavelengths (<0.73820Å), the attenuation coefficients are consistently higher. This discrepancy is most likely due to other scattering processes.

As with the silicon and germanium, plots of log (I) versus beam path length are not always linear. In fact, most of the plots start out linear as viewed from left to right. Then the slopes change gently so that the entire plot looks nonlinear. For the L_1, $L\alpha_1$, $L\beta_1$, and $L\gamma_1$ wavelengths, this is not entirely true. These plots start out linear from the left. Then there is a dip which appears to be wavelength dependent. The most interesting aspect of all these plots is that the final slopes of all the curves for all of the wavelengths appear to be the same.

Conclusions

The discrepancies in the reported attenuation coefficients for the temperature dependent data follow a definite trend. Four of the wavelengths for which questionable attenuation coefficients are reported are the second and third harmonics of the $L\alpha_1$ and $L\beta_1$ lines. This may indicate the possibility of an electronics problem with the counters or the single-channel analyzers. Human error should also be considered. At this time, no physical reasons are offered for these discrepancies. Clearly, the data which pertains to these questionable results must be taken again before any conclusions are made.

The change in linearity of the plots of log (I) versus beam path length cannot be easily explained. One may argue, however, that the curvature of these plots is due to increased scattering of the beam within the basal planes of HOPG as the crystal is rotated. This does not entirely explain the unreasonable attenuation coefficients obtained for HOPG at smaller wavelengths.

CHAPTER 6

Recommendations for Further Studies

In this investigation, it has been demonstrated that one may obtain information about attenuation coefficients by using the simple method described above. One may conclude that most of the attenuation coefficients measured in this study are reasonable since they follow the same functional dependence on the wavelength as those which have been published elsewhere (see Figures 4.3, 4.6, and 5.2 for other references). This is especially true for the perfect crystals in the thickness regime used during the data analysis.

The importance of this work is that the attenuation coefficient changes for different regions of beam path lengths in the same crystal. This has a profound effect on any measurements or calculations which rely on accurate attenuation coefficients. Physically, the nature of this change is not yet understood. The possibility of simultaneously measuring both transmitted and reflected beams would increase insight into the physical processes involved. Intensities calculated from the reflected and transmitted beam could be compared so that one may deduce the nature of other scattering processes through conservation laws: namely, conservation of photon number.

It would also be instructive to learn the nature of the attenuation coefficients derived from the reflected beam in the region where the attenuation coefficient changes as measured by the transmitted beam.

Measurements should be made with amorphous varieties of the materials

used in this study. This would clear up any ambiguities as to whether or not the change in attenuation coefficient for the thicker crystals is due to dynamical effects.

Finally, accurate measurements are needed to determine the relation between the effective crystal thickness relative to the beam and the point where this change in attenuation coefficients occur as a function of wavelength. A study of this type will permit one to know where care should be exercised in measuring intensities of reflected or transmitted beams for large effective crystal thickness.

BIBLIOGRAPHY

U. W. Arndt and B. T. M. Willis, Single Crystal Diffractometry, (University Press, Cambridge, 1966).

B. W. Batterman, and D. R. Chipman and J. J. DeMarco, Phys. Rev. 122, 68 (1961).

B. W. Batterman, and H. Cole, Rev. Mod. Phys. 36, 681 (1964).

P. R. Bevington, Data Reduction and Error Analysis for the Physical Sciences (McGraw-Hill, New York, 1969).

L. D. Calvert, R. C. G. Killean and A. Mc L. Mathieson, Acta Cryst. A32, 648 (1976).

R. Chen, P. Trucano and R. F. Stewart, Acta Cryst. A33, 823 (1977).

D. T. Cromer, Acta Cryst. 18, 17 (1965).

P. H. Dederichs, Physik Kondens. Materie 5, 347 (1966).

C. Ghezzi, A. Merlini and S. Pace, Phys. Rev. B4, 1833 (1971).

M. D. Giardino and A. Merlini, Z. Naturforsch. 28a, 1360 (1973).

G. Grimvall and E. Persson, Acta Cryst. A25, 417 (1969).

G. W. Grodstein, in X-ray Attenuation Coefficients From 10 keV to 100 MeV, Natl. Bur. Std. Circular 583 (U.S. GPO, Washington, D.C., 1957).

C. R. Hall and P. B. Hirsch, Proc. Roy. Soc. A286, 158 (1965).

W. C. Hamilton, Statistics in Physical Science (Ronald Press, New York, 1964).

G. Hildebrandt, J. D. Stevenson, and H. Wagenfeld, Z. Naturforsch. 28a, 588 (1973).

H. Hönl, Ann. Phys. Lpz. 5, 625 (1933).

R. Hosemann and S. N. Bagchi, Direct Analysis of Diffraction by Matter (Interscience Publishers Inc., New York, 1962).

International Tables for X-ray Crystallography (Kynoch Press, Birmingham, 1974), Vol. IV.

R. W. James, The Optical Principles of the Diffraction of X-rays, Third Edition (Bell, London, 1962. Reprinted by Ox Bow Press, Woodbridge, Connecticut, 1982).

C. Kittel, Introduction to Solid State Physics, Fourth Edition (John Wiley and Sons, Inc., New York, 1971).

D. W. Marquardt, J. Soc. Appl. Math. 11, 431 (1963).

R. T. McGinnies, in X-ray Attenuation Coefficients From 10 keV to 100MeV, Natl. Bur. Std. Supplement to Circular 583 (U.S. GPO, Washington, D.C., 1959).

E. W. Pike, J. Appl. Phys. 12, 206 (1941).

Z. G. Pinsker, Dynamical Scattering of X-rays in Crystals (Springer-Verlag, New York, 1978).

H. Sano, K. Ohtaka and H. Ohtsuki, J. Phys. Soc. Japan 27, 1254 (1969).

L. H. Schwartz, and J. B. Cohen, Diffraction from Materials (Academic Press, New York, 1977).

J. -L. Staudenmann, M. Sandholm, L. D. Chapman and G. L. Liedl, To be published in Nuclear Instruments and Methods (1984).

L. P. Tarasov and B. E. Warren, J. Chem. Phys. 4, 236 (1936).

H. Wagenfeld, Phys. Rev. 144, 216 (1966).

ACKNOWLEDGMENTS

There are many people who deserve my sincerest thanks for their help in this project. Jim Flatten provided some of the computer plotting routines. Equipment maintenance was handled by Mike Sandholm. Dr. Wayne Decker initiated the measurements of HOPG as a function of temperature. Alka Garg deserves special credit for her suggestions on improving the computer program NLS and her help with some of the data analysis. Finally, I would like to give my warmest appreciation and thanks to my advisor, Dr. Jean-Louis Staudenmann, who assisted me in every aspect of this project.

APPENDIX A

Data Analysis Method

An integral part of this work was the development of a FORTRAN computer program for nonlinear least-squares fit of a model to the data. The method used in the program to fit the parameters in the model to the data is the method of maximum neighborhood developed by D. W. Marquardt (1963) (see also, Bevington, 1969).

The method of maximum neighborhood performs an optimum interpolation between the Taylor series method and the gradient method, the interpolation being based upon the maximum neighborhood in which the truncated Taylor series gives an adequate representation of the nonlinear model.

Both the Taylor series method and the gradient method are inadequate by themselves for model fitting. In the Taylor series method, the model is expanded as a Taylor series and corrections to the several parameters are calculated at each iteration based on the assumption of local linearity. This method, while it converges rapidly near a local minimum of χ^2 (a goodness of fit parameter which will be defined later), will diverge if the initial model is not near a local minimum of χ^2. Even if near a local minimum failure to converge is not uncommon. The gradient method usually involves stepping off from the current trial parameter values in the negative gradient of χ^2. The problem with this method is the extremely slow convergence after a few iterations.

In the following paragraphs, the method of maximum neighborhood is developed.

Let the model to be fitted to the data be

$$E(y) = f(x_1, x_2, \ldots, x_m; a_1, a_2, \ldots, a_k) \tag{A1}$$

where $x_1, x_2, \ldots, x_m$ are independent variables, $a_1, a_2, \ldots, a_k$ are the population values of k parameters, and E(y) is the expected value of the dependent variable y. Let the data points be denoted by

$$(Y_i, X_{1i}, X_{2i}, \ldots, X_{mi}) \quad i = 1, 2, \ldots, n. \tag{A2}$$

The problem is to compute those estimates of the parameters which minimize

$$\chi^2 = \sum_{i=1}^{n} (1/\sigma_i)^2 (Y_i - f_i)^2 \tag{A3}$$

where f_i is the value of y_i predicted by (A1) at the i^{th} data point and σ_i is the uncertainty in the data point Y_i.

We can expand the fitting function f to first order in a Taylor's expansion as a function of the parameters a_j.

$$f(x_i, \underline{a} + \delta\underline{a}) = f_i(x, \underline{a}) = \sum_{j=1}^{k} \frac{\partial f_i}{\partial a_j} \delta a_j \tag{A4}$$

The derivatives may be calculated by

$$\frac{\partial f_i}{\partial a_j} = \frac{f_i(a_j + \Delta a_j) - f_i(a_j - \Delta a_j)}{2\Delta a_j} \tag{A5}$$

To this approximation, χ^2 can be expressed as a linear function of the parameter increments and therefore $\delta\underline{a}$ can be found by the standard least-squares method of setting $(\partial\chi^2/\partial\,\delta a_j) = 0$ for all j. Taking the appropriate derivatives a set of k simultaneous equations are obtained

$$\beta_l = \sum_{j=1}^{k} \delta a_j \alpha_{jl} \qquad l = 1, 2, \ldots, k \tag{A6}$$

where

$$\beta_l = \frac{1}{2} \frac{\partial\chi^2}{\partial a_l} = \sum_{i=1}^{n} (1/\sigma_i)^2 (y_i - f_i) (\partial f_i/\partial a_l) \tag{A7}$$

and

$$\alpha_{jl} \simeq \sum_{i=1}^{n} (1/\sigma_i)^2 (\partial f_i/\partial a_j) (\partial f_i/\partial a_l) \tag{A8}$$

The solution of which may be found quite easily through matrix methods. If Equation A4 were expanded to second order in δa_j, we would see that Equation A8 is a first order approximation to the curvature matrix

$$C_{jl} = \frac{1}{2} \frac{\partial^2 \chi^2}{\partial a_j \partial a_l} \tag{A9}$$

which defines the curvature of χ^2 in the parameter space.

Up till now, the method shown is simply a Taylor series method. To combine the two methods, the diagonal terms of the curvature matrix

α are increased by a factor λ which controls the interpolation of the algorithm between the Taylor and gradient methods. The matrix Equation A6 becomes

$$\beta_l = \sum_{j=1}^{k} \delta a_j \, \alpha'_{jl} \tag{A10}$$

where

$$\alpha'_{jl} = \begin{cases} \alpha_{jl} \, (1 + \lambda) & \text{for } j = l \\ \alpha_{jl} & \text{for } j \neq l \end{cases} \tag{A11}$$

The solutions then for the parameter increments δa_j are simply

$$\delta a_j = \sum_{l=1}^{k} \beta_l \varepsilon'_{jl} \tag{A12}$$

where the matrix ε' is the inverse of the matrix α' whose elements are given in A11.

The strategy then to fit the model to the data is (Bevington, 1969):

1. Compute χ^2 (a).
2. Start with $\lambda = 0.001$.
3. Compute $\delta\underline{a}$ and χ^2 $(\underline{a} + \delta\underline{a})$ with this λ.
4. If χ^2 $(\underline{a} + \delta\underline{a}) > \chi^2(\underline{a})$, increase λ by a factor of 10 and repeat step 4.
5. If χ^2 $(\underline{a} + \delta\underline{a}) < \chi^2(\underline{a})$, decrease λ by a factor of 10, consider $\underline{a}' = \underline{a} + \delta\underline{a}$ to be a starting point, and return to step 3 with $\underline{a} = \underline{a}'$.

There are variations to this. For instance, on occasion in problems where the correlations among the parameter-estimates are high (>0.99), it can happen that λ will increase to unreasonably high values. In this case, it has been found best to alter step 5 so that $a'_j = a_j + \kappa \delta a_j$ where κ is some value less than one but greater than zero.

If λ is very small, Equation A10 is similar to Equation A6, and the solutions obtained are similar to those obtained through the Taylor expansion method. If λ is very large, the diagonal terms of the curvature matrix dominate and the matrix equation degenerates into k separate equations

$$\beta_j = \lambda \delta a_j \alpha_{jj} \tag{A13}$$

which will yield increments δa_j in the same direction as the gradient of β_1 in Equation A7.

One advantage of combining these two methods into one algorithm is that the expansion need only be valid in the immediate neighborhood of the minimum χ^2. Thus, only the simple first-order expansion is necessary and the first order approximation for the curvature matrix need be used.

As with most standard least-squares methods, it is possible for the model to converge to the improper local minima of χ^2. This is especially true of models which are based on periodic-like functions. Thus there is a need for human interaction during execution of any computer program which uses this method with periodic-like functions. This is to ensure that the parameters obtained are physically meaningful.

APPENDIX B

Portions of the FORTRAN program NLS used to perform the least-squares analysis in this work.

```
C
C     PROGRAM NLSFIT
C
C     PURPOSE
C        TO DO A GENERALIZED LEAST SQUARES
C
C     DESCRIPTION OF PARAMETERS
C        OBS    - ARRAY OF DATA POINTS (OBSERVED DEPENDENT VARIABLE)
C        XVALUE - ARRAY OF DATA POINTS (INDEPENDENT VARIABLE)
C        PARAM  - ARRAY OF PARAMETERS FOR FITTING FUNCTION
C                 SOME OR ALL OF WHICH CAN BE OPTIMIZED BY THIS PROGRAM
C        NXFLAG - ARRAY OF FLAGS WHICH DETERMINE WHICH PARAMETERS WILL
C                 BE MODIFIED BY THIS PROGRAM
C                    1 = PARAMETER INCLUDED IN L.S.
C                    0 = PARAMETER NOT INCLUDED IN L.S.
C        NILS     ARRAY OF FLAGS FOR DATA POINTS
C                    NILS .LE. 0  => NOT INCL. IN L.S.
C                    NILS .GT. 0  => INCL. IN L.S.
C                    IABS(NILS) .EQ. 2  => POINT HAS BEEN MODIFIED
C                 NILS SETS UP REGIONS OF INTEREST IN THE WHOLE DATA
C        SIGMA    ARRAY OF STANDARD DEVIATIONS OF OBS
C                 NOT USED IN THIS VERSION AS DEFINED.  CAN BE MODIFIED
C                 BY INTRODUCING A NEW ARRAY AND REPLACING SIGMA IN THE
C                 MAIN PART OF THIS ROUTINE BY THE NEW ARRAY.  SEE
C                 COMMENTS IN BODY OF THIS ROUTINE, SIGMA MAY THEN BE
C                 USED AS INDICATED.
C        CALC     ARRAY OF CALCULATED VALUES OF THE FITTING FUNCTION
C        WEIGH    ARRAY OF WEIGHTS OF OBS
C        IFLAG    ARRAY OF FLAGS FOR VARIOUS SUBROUTINES
C                 (1) NUMBER OF PARAMETERS TO BE FITTED --SETFUN
C                 (2) MAX NO. OF PARAMETERS IN FUNCTION --SETFUN
C                 (3) BEGINNING INDEX OF DATA FOR NLSFIT--LSPARM
C                 (4) ENDING INDEX OF DATA FOR NLSFIT   --LSPARM
C                 (5) CONTROL FLAG                      --NLSFIT
C                     0= NEW JOB, 1= SAME DATA, 2= MORE DATA
C                 (6) PRINT FLAG FOR SUBROUTINE TITRE   --******
C                 (7) FILE OPERATION   OR SUBFILE       --COLLCT
C                 (8) COUNTER NUMBER                    --COLLCT
C                 (9) PRINT FLAG FOR SUBROUTINE RCHISQ  --******
C                (10) PRINT FLAG FOR SUBROUTINE TITRE   --******
C                (11) SMOOTHING FLAG                    --LSPARM
C                     0= NONE, 1= 3-POINT, 2= 5-POINT
C                (12) MAX DATA INDEX READ IN            --COLLCT
```

```
C                (13) NO. CYCLES OF REFINEMENT           --LSPARM
C                (14) PLOTTING FLAG                      --LSPARM
C                     0= NONE, 1= AT END, 2=EACH CYCLE
C                (15) PLOTTING FLAG                      --LSPARM
C                     0= PROG CHOOSE MAX SCALE FOR PLOT
C                     1= NOT
C                (16) PLOT SCALE INDEX IF IFLAG(15)= 1   --LSPARM
C                (17) 0= CHI COMPARE, 1= NOT             --LSPARM
C                (18) 0= PRINT MATRIX OF COEF. & INVRT   --LSPARM
C                     1= NOT
C                (19) WEIGHT FLAG                        --LSPARM
C                     0= NO WEIGHT
C                     1= STATISTICAL (1/OBS)
C                     2= INSTRUMENTAL (1/(SIGMA*SIGMA))
C                (20) 0= TRUNCATE CALC VALUES            --LSPARM
C                     1= NOT
C                (21) NORMALIZATION OF DAT FLAG          --LSPARM
C                     0= NO NORMALIZATION
C                     1= NORMALIZE OBS TO 10^6
C                     2= NORMALIZE CALC TO 10^6
C                     3= NORMALIZE BOTH TO 10^6
C                (22) PRINT FLAG FOR SUBROUTINE CURFIT   --LSPARM
C                     0= LONG OUTPUT
C                     1= SHORT OUTPUT
C
C     SUBROUTINES CALLED BY NLSFIT
C        COLLCT  CORREL  CURFIT  EXIT     FISTAT  FIXIT    FUNCTN  LSPARM
C        NOTINC  PAGING  PLOTV   RCHISQ   SETFUN  SETUP    SMOOTH  TABLE
C        TITRE   WEIGHT
C
C     COMMENTS
C       PLEASE NOTE THAT SUBROUTINE SETUP IS NOT REQUIRED TO RUN THIS
C       PROGRAM.  IT WAS INITIALLY USED TO SET ALL VARIABLES AND FLAGS
C       TO SPECIFIC VALUES.  IT ALSO TESTS THE SYSTEM CLOCK TO SEE IF
C       IT IS RUNNING. IF NO CLOCK IS PRESENT OR THE CLOCK IS OFF THE
C       PROGRAM WILL HANG. REMOVING THIS SUBROUTINE AND CALL STATEMENT
C       WILL NOT AFFECT THE OPERATION OF THIS PROGRAM.
C
C       ALSO NOTE THAT THE SUBROUTINE TITRE USES THE FORTRAN SUBROUTINES
C       CALLED "TIME" AND "DATE".  THESE MAY BE EDITED OUT IF THE SYSTEM
C       HAS NO CLOCK.
C
C       THE TIME FUNCTIONS ARE ONLY AN AID TO THE OPERATOR.
C
C
C
      PROGRAM NLSFIT
      DIMENSION IFLAG(30),CALC(256),OBS(256),SIGMA(256),XVALUE(256)
```

```
      DIMENSION WEIGH(256),NXFLAG(20),PARAM(20),NILS(256)
      REAL*8 ARRAY(20,20),CHISQ(5),RLAST
      LOGICAL*1 DAY(9),TITLE(80),XLABEL(20),YLABEL(20),BEL
      LOGICAL*1 FILNAM(15),NUL,CONTNT(80),NEWLA(20),IANS
      COMMON IFLAG,LINE,NPAGE
      COMMON /DAT/CALC,OBS,NILS
      COMMON /FDAT/NXFLAG,PARAM,XVALUE
      COMMON /WAY/WEIGH
      COMMON /PIERR/SIGMA,CHISQ
      COMMON /MISC/FRAC,RLAST
      COMMON /LABELS/XLABEL,YLABEL
      COMMON /TOP/DAY,TITLE,FILNAM,CONTNT
      COMMON /CURCOR/ARRAY
      COMMON /VARI/FLAMDA
      DATA XLABEL/20*''/, YLABEL/20*''/, TITLE/80*''/
      DATA IFLAG/30*0/,PARAM/20*.1
      DATA NILS/256*1/
      DATA NEWLA/'D','I','F','F',':','','O','B','S',' ',
     +           'C','A','L','C',' ','',' ',' ',' ',' '/
      NUL= ,FALSE.
      IFLAG(5)= 0
      TYPE 100
30210 FLAMDA= 0.001
      ICYCLE= 0
      IF (IFLAG(5) .NE. 1) GO TO 30290
      TYPE 107
      ACCEPT 530,IANS
      IF (IANS .NE. 'N') GO TO 30710
30290 TYPE 102
      ACCEPT 505,(TITLE(I), I= 1, 50)
      IF (IFLAG(5)-1) 30310,30430,30310
30310 DO 80320 J= 1, 256
80320 NILS(J)= 1
      NPAGE=1
      LINE= 4
C
C      HERE IS THE SUBROUTINE SETUP
C      THIS MAY BE REMOVED AS INDICATED IN EARLIER COMMENTS
C
      CALL SETUP
C
C      END OF SETUP ROUTINE COMMENTS
C
      CALL COLLCT
      IFLAG(11)= 0
      NUL= .FALSE.
      DO 80340 J= 55, 71
80340   TITLE(J)=
      TYPE 105
      ACCEPT 510,PHAZE
```

```
      DO 80390 I= 1, IFLAG(4)
80390    XVALUE(I)= XVALUE(I)+PHAZE
      CALL TITRE
      CALL PLOTV(1,OBS,OBS,XVALUE,IFLAG(3),IFLAG(4),IFLAG(15),IFLAG(16),
     +           XLABEL,YLABEL)
      CALL TITRE
30430 IF(IFLAG(5) .EQ. 1) TYPE 109
      TYPE 104
      ACCEPT 530,IANS
      IF (IANS .EQ. 'N') GO TO 30490
      CALL FIXIT
      CALL TITRE
30490 CALL LSPARM
      IF (IFLAG(21) .NE. 1) GO TO 30590
      YMAX= -1.0E+30
      DO 80560 I= IFLAG(3),IFLAG(4)
80560    YMAX= AMAX1(YMAX,OBS(I))
      ANORM= 1.0E+06/YMAX
      DO 80580 I= IFLAG(3), IFLAG(4)
80580    OBS(I)= OBS(I)*ANORM
30590 IF (IFLAG(11) .EQ. 0 .OR. NUL) GO TO 30640
      CALL SMOOTH
      NUL= .TRUE.
      CALL TITRE
      CALL PLOTV(1,OBS,OBS,XVALUE,IFLAG(3),IFLAG(4),IFLAG(15),IFLAG(16),
     +           XLABEL,YLABEL)
30640 CALL TITRE
      IF (IFLAG(5) .EQ. 1) TYPE 109
      TYPE 108
      ACCEPT 530,IANS
      IF (IANS .EQ. 'N') GO TO 30710
      CALL NOTINC
      CALL TITRE
30710 CALL SETFUN
      TYPE 110
      ACCEPT *,FRAC
      LINE= LINE+4
      DO 80750 J= IFLAG(3), IFLAG(4)
         JSUB= J
80750    CALC(JSUB)= FUNCTN(JSUB)
      IF (IFLAG(5) .NE. 1) GO TO 30800
      TYPE 103
      ACCEPT 530,IANS
      IF (IANS .NE. 'Y') GO TO 30820
30800 IFLAG(6)= 4
      CALL TABLE
30820 IF (IFLAG(19) .NE. 0) CALL WEIGHT
      IFLAG(9)= 2
      CALL RCHISQ
      IF (SNGL(CHISQ(5)) .LT. 0.075) GO TO 30980
```

```
      CALL TITRE
      TYPE 115
30880 LINE= LINE+3
      CALL PAGING
      TYPE 120
      ACCEPT 520,NUM
      IF (NUM .EQ. 0) GO TO 30980
      TYPE 125,NUM,PARAM(NUM)
      ACCEPT *,PARAM(NUM)
      IFLAG(9)= 2
      CALL RCHISQ
      IF (SNGL(CHISQ(5)) .GE. 0.075) GO TO 30880
30930 RLAST= CHISQ(5)
      ICYCLE= ICYCLE+1
      IF (ICYCLE .EQ. 1 .AND. IFLAG(22) .EQ. 1) CALL TITRE
      IF (ICYCLE .EQ. IFLAG(13)) IFLAG(22)= 0
      IF (IFLAG(22) .EQ. 1) GO TO 31020
      CALL TITRE
      TYPE 130,ICYCLE,IFLAG(13)
31020 CALL CURFIT
      DO 31050 J= IFLAG(3), IFLAG(4)
         JSUB= J
31050    CALC(JSUB)= FUNCTN(JSUB)
      IF (ICYCLE .NE. IFLAG(13) .OR. IFLAG(21) .LE. 1) GO TO 31160
      YMAX= -1.0E+30
      DO 81100 I= IFLAG(3), IFLAG(4)
      YMAX= AMAX1(YMAX,CALC(I))
81100    IF (IFLAG(21) .EQ. 3) YMAX= AMAX1(YMAX,OBS(I))
      ANORM= 1.0E+06/YMAX
      PARAM(1)= PARAM(1)*ANORM
      DO 81150 I= IFLAG(3), IFLAG(4)
      CALC(I)= CALC(I)*ANORM
81150 OBS(I)= OBS(I)*ANORM
31160 IF (IFLAG(14) .EQ. 2) CALL TITRE
      IF (IFLAG(14) .EQ. 2) CALL PLOTV(2,OBS,CALC,XVALUE,IFLAG(3),
     +               IFLAG(4), IFLAG(15),IFLAG(16),XLABEL,YLABEL)
31190 IF (ICYCLE .GE. IFLAG(13)) GO TO 31210
      IF ((CHISQ(5)-RLAST) .LT. 0.5E-07) GO TO 30980
31210 RLAST= CHISQ(5)
      CALL CORREL
      IFLAG(6)= 1
      CALL TABLE
      IFLAG(6)= 0
      IF (IFLAG(14) .NE. 1) GO TO 31310
      CALL TITRE
      CALL PLOTV(2,OBS,CALC,XVALUE,IFLAG(3),
     +               IFLAG(4), IFLAG(15),IFLAG(16),XLABEL,YLABEL)
      CALL TITRE
31310 IF (IFLAG(14) .EQ. 0) GO TO 30360
C
```

```
C     HERE IS WHERE THE SIGMA ARRAY IS USED NOT IN THE
C     MANNER OF ITS DESCRIPTION.  THIS MAY BE CHANGED
C     IN ACCORDANCE TO EARLIER COMMENTS ABOVE.
C
      DO 81330 J= IFLAG(3), IFLAG(4)
81330    SIGMA(J)= OBS(J)-CALC(J)
      CALL PLOTV(3,SIGMA,CALC,XVALUE,IFLAG(3),IFLAG(4),
     +           IFLAG(15),IFLAG(16),XLABEL,NEWLA)
C
C      END OF SIGMA ARRAY COMMENTS.
C
30360 CALL TITRE
      CALL FISTAT
      CALL TITRE
      TYPE 135
      ACCEPT 530,IANS
      IF (IANS .NE. 'Y') CALL EXIT
      TYPE 101
      ACCEPT 500,IFLAG(5)
      GO TO 30210
C
                              FORMAT STATEMENTS
C
  100 FORMAT(1H1,'NLSFIT V02:02   double precision in this version',
     +       /,3X,'              1 overlay region with 11 segments',
     +       /,5X,'            Latest version November 9, 1983',/,/)
  101 FORMAT(1H0,10X,'Enter 0= New Job, 1= Same data, 2=
     +         ,'More data from same file',T75,$)
  102 FORMAT(1H0,10X,'Enter the General Title ',5X,$)
  103 FORMAT(1H0,10X,'Do you want an initial table ? ..(Y/N)..  ',$)
  104 FORMAT(1H0,10X,'Do you want to change specific points ',/,
     +        1H ,10X,'in the data ?  ...(Y/N)...  ',10X,$)
  105 FORMAT(1H0,10X,'Enter zero (or phase) angle',38X,$)
  107 FORMAT(1H0,10X,'Do you want to keep everything the same',/,
     +       11X,'and start from and of the last cycle ? ..(Y/N)..',/,
     +       10X,$)
  108 FORMAT(1H0,10X,'Do you want to exclude some regions of data ',/,
     +        1H ,10X,'in the L.S. Fit ?  ...(Y/N)...  ',10X,$)
  109 FORMAT(1H0,10X,'Remember that the old values will be ',/,
     +           11X,'kept in the following question, ')
  110 FORMAT(1H0,10X,'Enter fraction (=DER. Step/Unknown):',T75,$)
  115 FORMAT(1H0,10X,'OPTIMIZATION OF SOME UNKNOWNS ',/)
  120 FORMAT(1H0,10X,'Enter 0= continue #= No. of Param. to change',
     +       T75,$)
  125 FORMAT(16X,'Old value of parameter # ',13,' = ',1PG17,10,
     +          Enter new value  ',T75,$)
  130 FORMAT(1X,' CYCLE #',13,' OF ',13,/)
  135 FORMAT(1H0,10X,'Do you want to do it again ?  ...(Y/N)...  ',
     +       5X,$)
  500 FORMAT(I1)
```

```
  505 FORMAT(50A1)
  530 FORMAT(1A1)
  510 FORMAT(F6.4)
  520 FORMAT(I2)
  525 FORMAT(E11.4)
  550 FORMAT(1X,F9.1,3X,F7.3,3X,F10.5)
      END



C
C      SUBROUTINE CURFIT
C
C     PURPOSE
C        TO MAKE A LEAST-SQUARES FIT TO A NON-LINEAR FUNCTION
C        WITH A LINEARIZATION OF THE FITTING FUNCTION
C
C     USAGE
C        CALL CURFIT
C
C     DESCRIPTION OF PARAMETERS
C        PARAM  - ARRAY OF PARAMETERS FOR THE FITTING FUNCTION
C        OBS    - ARRAY OF DATA POINTS (OBSERVED DEPENDENT VARIABLE)
C        SIGMA  - ARRAY OF STANDARD DEVIATIONS OF OBS
C        IFLAG  - ARRAY OF FLAGS FOR VARIOUS SUBROUTINES
C        XVALUE - ARRAY OF DATA POINTS (INDEPENDENT VARIABLES)
C
C     SUBROUTINE AND FUNCTION SUBPROGRAMS REQUIRED
C        FUNCTN(I)
C        RCHISQ
C        DERIVA(I,DERIV)
C        MATINV(ARRAY,NORDER,DET)
C        MATRIX
C        TITRE
C        PAGING
C        PTSCAN
C
C     COMMENTS:
C       SET FLAMDA= 0.001 AT BEGINNING OF SEARCH
C        SEE DATA REDUCTION AND ERROR ANALYSIS FOR THE PHYSICAL SCIENCES
C        BY PHILIP R. BEVINGTON, MCGRAW-HILL.  THIS BOOK WILL EXPLAIN
C        HOW THIS ROUTINE WORKS IN DETAIL.
C
C
C
      SUBROUTINE CURFIT
      DIMENSION XVALUE(256),OBS(256),CALC(256),NILS(256)
      REAL*8 ALPHA(20,20),BETA(20),B(20),DERIV(20)
      DIMENSION IFLAG(30),PARAM(20)
```

```
      DIMENSION OLD(20),WEIGH(256),NXFLAG(20),SIGMA(256)
      REAL*8 ARRAY(20,20),CHISQ(5),RLAST
      COMMON IFLAG,LINE,NPAGE
      COMMON /DAT/CALC,OBS,NILS
      COMMON /FDAT/NXFLAG,PARAM,XVALUE
      COMMON /PIERR/SIGMA,CHISQ
      COMMON /WAY/WEIGH
      COMMON /CURCOR/ARRAY
      COMMON /MISC/FRAC,RLAST
      COMMON /VARI/FLAMDA
      FLAMDA= 0.001
      NLAMDA= 0
      DATA BETA/20*0.0D+00/ ALPHA/400*0.0D+00/ WEIGH/256*1./
      DATA DERIV/20*0.0D+00/
      IF (IFLAG(19) .NE. 0) CALL WEIGHT
      DO 80340 I= IFLAG(3), IFLAG(4)
         IF (NILS(I) .LE. 0) GO TO 80340
         ISUB= I
         CALL DERIVA(ISUB,DERIV)
         L= 0
         DO 80330 J= 1, IFLAG(2)
            IF (NXFLAG(J) .EQ. 0) GO TO 80330
            L= L+1
            BETA(L)= BETA(L)+WEIGH(I)*(OBS(I)-FUNCTN(ISUB))*DERIV(L)
            M= 0
            DO 80320 K= 1, J
               IF (NXFLAG(K) .EQ. 0) GO TO 80320
               M= M+1
               ALPHA(L,M)= ALPHA(L,M)+WEIGH(I)*DERIV(L)*DERIV(M)
80320          CONTINUE
80330       CONTINUE
80340    CONTINUE
      DO 80370 J= 1, IFLAG(1)
         DO 30370 K= 1, J
80370       ALPHA(K,J)= ALPHA(J,K)
      IFLAG(9)= 0
      CALL RCHISQ
      PRECHI= SNGL(CHISQ(5))
30410 DO 80440 J= 1, IFLAG(1)
         DO 80430 K= 1, IFLAG(1)
80430       ARRAY(J,K)= ALPHA(J,K)/DSQRT(ALPHA(J,J)*ALPHA(K,K))
80440    ARRAY(J,J)= 1.0+FLAMDA
      CALL MATINV(ARRAY,IFLAG(1),DET)
      DO 80460 J= 1, IFLAG(2)
80460    OLD(J)= PARAM(J)
      L= 0
      DO 80580 J= 1, IFLAG(2)
         IF (NXFLAG(J) .EQ. 0) GO TO 80580
         L= L+1
         B(L)= PARAM(J)
```

```
         M= 0
         DO 80570 K= 1, IFLAG(2)
            IF (NXFLAG(K) .EQ. 0) GO TO 80570
            M= M+1
            B(L)= B(L)+BETA(M)*ARRAY(L,M)/DSQRT(ALPHA(L,L)*ALPHA(M,M))
80570       CONTINUE
80580    CONTINUE
      L= 0
      DO 80640 J= 1, IFLAG(2)
         IF (NXFLAG(J) .EQ. 0) GO TO 30640
         L= L+1
         PARAM(J)= B(L)
80640    CONTINUE
      IFLAG(9)= 0
      CALL RCHISQ
      IF (IFLAG(17) .GT. 0) GO TO 30740
      IF ((PRECHI-SNGL(CHISQ(5))) .GE. 0) GO TO 30740
      FLAMDA= FLAMDA*10.0
      NLAMOA= NLAMDA+1
      DO 80720 J= 1, IFLAG(2)
80720    PARAM(J)= OLD(J)
      GO TO 30410
30740 IF (IFLAG(22) .EQ. 1) GO TO 30890
      IFLAG(6)= 5
      IFLAG(10)= 1
      CALL TITRE
      LINE= LINE+3
      L= 0
      DO 80880 J= 1, IFLAG(2)
         IF (NXFLAG(J) .EQ. 0) GO TO 80370
         L= L+1
         CHANGE= PARAM(J)-OLD(J)
         STDEV= DSQRT(DABS(ARRAY(L,L)/ALPHA(L,L)))
         WRITE(7,125) J,OLD(J),CHANGE,PARAM(J),STDEV
         GO TO 80880
80870       WRITE(7,120) J,PARAM(J),NXFLAB(J)
80880    CONTINUE
30890 WRITE(7,130) FLAMDA,NLAMDA
30900 IF (IFLAG(19) .EQ. 0) GO TO 30930
      WRITE(7,135) CHISQ(5),RLAST
      GO TO 30940
30930 WRITE(7,140) CHISQ(5),RLAST
30940 IF (IFLAG(22) .EQ. 1) GO TO 30980
      IFLAG(9)= 3
      CALL RCHISQ
      CALL PTSCAN
      IFLAG(6)= 0
30980 DO 81030 J= 1, IFLAG(1)
         DO 81020 K= 1, IFLAG(1)
81020       ARRAY(J,K)= ALPHA(J,K)/DSQRT(ALPHA(J,J)*ALPHA(K,K))
```

```
81030    ARRAY(J,J)= 1.00+00
      IF (IFLAG(18) .NE. 0 .OR. IFLAG(22) .EQ. 1) GO TO 31110
      CALL TITRE
      WRITE(7,100)
      CALL MATRIX
      NLINE= (IFLAG(1)*2)+7
      LINE= LINE+(2*NLINE)
      IF (LINE .GT. 80) CALL TITRE
31110 CALL MATINV(ARRAY,IFLAG(1),DET)
      IF (IFLAG(18) .NE. 0 .OR. IFLAG(22) .EQ. 1) RETURN
      WRITE(7,145)
      CALL MATRIX
      RETURN
C
                          FORMAT STATEMENTS
C
  100 FORMAT(1H0,'MATRIX OF COEFFICIENTS')
  120 FORMAT(1H0,10X,I3,7X,1PG14.7,7X,I1)
  125 FORMAT(1H0,10X,I3,7X,1PG14.7,6X,1PG14.7,6X,1PG14.7,6X,1PG12.5)
  130 FORMAT(1H0,10X,'FINAL FLAMDA = ',1PG16.9,SX,'( CHANGED',
 +           I4,' TIMES )',/)
  135 FORMAT(29X,'WEIGHTED R-FACTOR = ',1PG17.10,/,
 +           8X,'FOR PRECEEDING CYCLE WEIGHTED R-FACTOR = ',
 +            1P017.10,/)
  140 FORMAT(29X,'UNWEIGHTED R-FACTOR = ',1PG17.10,/,
 +           8X,'FOR PRECEEDING CYCLE UNWEIGHTED R-FACTOR = ',
 +           1PG17.10,/)
  145 FORMAT(1H0,'INVERTED MATRIX')
      END
```

```
C
C      SUBROUTINE RCHISQ
C
C      PURPOSE
C         EVALUATE REDUCED CHI-SQUARE FOR FIT TO DATA
C         CHISQ= SUM[ (OBS-CALC)**2/SIGMA**2  ] / NDFREE
C
C      USAGE
C         CALL RCHISQ
C
C      DESCRIPTION OF PARAMETERS
C         OBS    - ARRAY OF DATA POINTS (OBSERVED DEPENDENT VARIABLES)
C         NPFLAG - PRINT FLAG SAME AS IFLAG(9)
C                  0= COMPUTATION ONLY
C                  1= COMPUTATION AND PRINT (CHISQ(I), I= 1, 4)
C                  2= COMPUTATION AND PRINT R-FACTOR(S) ONLY
```

```
C                  3= COMPUTATION AND PRINT CHI-SQUARE(S) ONLY
C        WEIGH  -  ARRAY OF WEIGHTS OF OBS
C        XVALUE -  ARRAY OF DATA POINTS (INDEPENDENT VARIABLE)
C        PARAM  -  ARRAY OF PARAMETERS FOR FITTING FUNCTION
C        CHISQ  -  ARRAY RETURNED TO CALLING PROGRAM UNIT
C                  (1)= UNWEIGHTED CHI-SQUARE
C                  (2)= WEIGHTED CHI-SQUARE
C                  (3)= UNWEIGHTED R-FACTOR
C                  (4)= WEIGHTED R-FACTOR
C                  (5)= CHISQ(3) IF IFLAG(19) = 0
C                     = CHISQ(4) IF IFLAG(19) > 0
C                       IFLAG(19) IS WEIGHTING SCHEME FLAG
C
C     SUBROUTINE AND FUNCTION SUBPROGRAMS REQUIRED
C        FUNCTN(I)
C
C     COMMENTS
C        NDFREE IS THE DEGREE OF FREEDOM
C        NOTE ALL COMPUTATIONS ARE DONE IN REAL*8
C
      SUBROUTINE RCHISQ
      DIMENSION OBS(256),WEIGH(256),XVALUE(256),PARAM(20),PARAM(20),NILS(256)
      DIMENSION IFLAG(30),CALC(256),NXLFAG(20),SIGMA(256)
      REAL*8 CHISQ(5),DELTSQ,UWCHI,WCHI,DELTA
      REAL*8 SDELSQ,SOBSSQ,SWDSQ,SWOBSQ
      COMMON IFLAG,LINE,NPAGE
      COMMON /WAY/WEIGH
      COMMON /FDAT/NXFLAG,PARAM,XVALUE
      COMMON /DAT/CALC,OBS,NILS
      COMMON /PIERR/SIGMA,CHISQ
      NPFLAG= IFLAG(9)
      DO 80140 J= 1, 5
         CHISQ(J)= 0.
80140 CONTINUE
      ICOUNT= 0
      SDELSQ= 0.
      SOBSSQ= 0.
      SWDSQ= 0.
      SWOBSQ= 0.
      DO 80330 J= IFLAG(3), IFLAG(4)
         IF (NILS(J) .LE. 0) GO TO 80330
         ICOUNT= ICOUNT+1
         JSUB= J
         FUN= FUNCTN(JSUB)
         IF (IFLAG(20) .EQ. 0) FUN= AINT(FUN+0.5)
         DELTA= OBS(J)-FUN
         DELTSQ= DELTA*DELTA
         SDELSQ= SDELSQ+DELTSQ
         SOBSSQ= SOBSSQ+OBS(J)*OBS(J)
         IF (IFLAG(19) .EQ. 0) GO TO 80330
```

```
         SWDSQ= SWDSQ+WEIGH(J)*DELTSQ
         SWOBSQ= SWOBSQ+WEIGH(J)*OBS(J)*OBS(J)
80330 CONTINUE
      NDFREE= ICOUNT-IFLAG(1)+1
      CHISQ(1)= SDELSQ/DBLE(FLOAT(NDFREE))
      CHISQ(3)= DSQRT(SDELSQ/SOBSSQ)
      UWCHI= DSQRT(CHISQ(1))
      IF (IFLAG(19) .EQ. 0) GO TO 30420
      CHISQ(2)= SWDSQ/DBLE(FLOAT(NDFREE))
      CHISQ(4)= DSQRT(SWDSQ/SWOBSQ)
      WCHI= DSQRT(CHISQ(2))
30420 GO TO (30540,30430,30490,30430),(NPFLAG+1)
30430 WRITE(7,100) NDFREE
      WRITE(7,100) SDELSQ,CHISQ(1),UWCHI
      LINE= LINE+2
      IF (IFLAG(19) .EQ. 0) GO TO 30490
      WRITE(7,120) SWDSQ,CHISQ(2),WCHI
      LINE= LINE+1
30490 IF (NPFLAG .EQ. 3) GO TO 30540
30490 IF (NPFLAG .EQ. 3) GO TO 30540
      WRITE(7,130) CHISQ(3)
      LINE= LINE+2
      IF (IFLAG(19) .EQ. 0) GO TO 30540
      WRITE(7,140) CHISQ(4)
      LINE= LINE+1
30540 CHISQ(5)= CHISQ(3)
      IF (IFLAG(19) .GT. 0) CHISQ(5)= CHISQ(4)
      RETURN
C
                          FORMAT STATEMENTS
C
  100 FORMAT(1HO,'(#OBS - #PARAM) = d.f. = ',110)
  110 FORMAT(1H ,'SUM [ (OBS-CALC)**2 ]  = ',1PG17.10,/,
     +       1H ,'UNWEIGHTED CHI-SQUARE  = ',1PG17.10,/,
     +       1H ,'UNWEIGHTED CHI         = ',1PG17.10)
  120 FORMAT(1H ,'SUM [ (OBS-CALC)**2 ]  = ',1PG17.10,/,
     +       1H ,'  WEIGHTED CHI-SQUARE  = ',1PG17.10,/,
     +       1H ,'  WEIGHTED CHI         = ',1PG17.10)
  130 FORMAT(1HO,'UNWEIGHTED R-FACTOR    = ',1PG17.10)
  140 FORMAT(1H ,'  WEIGHTED R-FACTOR    = ',1PG17.10)
      END




C
C        SUBROUTINE DERIVA(I,DERIV)
C
```

```
C         PURPOSE
C            TO CALCULATE DERIVATIVES OF AN ARBITRARY FUNCTION
C            FOR A LEAST SQUARES FIT.
C
C         PARAMETERS
C            DERIV   - ARRAY OF DERIVATIVES OF FUNCTION
C            I       - INDEX OF DATA POINT ABOUT WHICH DERIVATIVES ARE
C                      EVALUATED
C
C         FUNCTIONS REQUIRED
C            FUNCTN
C
C         COMMENTS
C            NOTE THAT CALCULATIONS ARE DONE IN DOUBLE PRECISION
C            ALSO NOTE THAT DELTA IS CONSTRAINED NOT TO BE EQUAL TO
C            ZERO.  THIS MAY LEAD TO SOME PROBLEMS WITH SOME FUNCTIONS.
C            IF DERIVA IS ZERO TOO MANY TIMES A SINGULAR MATRIX WILL
C            BE CREATED AND CURFIT WILL CRASH.
C
C            THE ABOVE WAS DONE FOR FNCT11.FOR.  THIS WAS SO THAT SOME
C            OF THE PARAMETERS MAY BE STARTED AT ZERO INSTEAD OF A FINITE
C            BUT SMALL NUMBER.
C
C            PLEASE NOTE THAT THE PARAMETERS ARE "SHUFFLED" ACCORDING TO
C            THE FLAGS NXFLAG.
C
C
C
      SUBROUTINE DERIVA(I,DERIV)
      DIMENSION XVALUE(256),PARAM(20),IFLAG(30),NXFLAG(20)
      REAL*8 RLAST,DERIV(20)
      COMMON IFLAG,LINE,NPAGE
      COMMON /FDAT/NXFLAG,PARAM,XVALUE
      COMMON /MISC/FRAC,RLAST
      IJK= 0
      DO 900 J= 1, IFLAG(2)
         IF (NXFLAG(J) .EQ. 0) GO TO 900
         IJK= IJK+1
         HOLD= PARAM(J)
    1    DELTA= PARAM(J)*FRAC
         IF (DELTA .EQ. 0.0) DELTA= 0.01
         PARAM(J)= HOLD+DELTA
         YFIT= FUNCTN(I)
         PARAM(J)= HOLD-DELTA
         FUN= FUNCTN(I)
         DIF= YFIT-FUN
         IF (DIF .NE. 0.) GO TO 3
         DERIV(IJK)= 0.0D+00
         GO TO 2
    3    DERIV(IJK)= DBLE(DIF)/DBLE(2.0*DELTA)
```

```
  2     PARAM(J)= HOLD
900 CONTINUE
    RETURN
    END
```

APPENDIX C

The Filter Method for Estimating the Incident Intensity of the X-ray Beam

For initial estimates of the incident intensity, I_o, a simple method was needed. The filter method was used to obtain these estimates. This method requires the use of at least two different materials. By using Equation 1.3 it is possible to determine I_o.

The intensity of the transmitted beam of x-rays is measured for the sample crystal at a particular orientation. This intensity is proportional to the incident intensity by

$$I_s = I_o T_s \tag{C1}$$

where I_s is the transmitted intensity due to the sample in the beam and $T_s = \exp(-\mu_s t_s)$. Here, μ_s is the absorption coefficient of the sample and t_s is the thickness of the sample which remains constant while performing this technique.

A filter is then put into the beam and the transmitted intensity is measured. The equation which relates this intensity to the incident intensity is

$$I_{sF} = I_o \exp(-\mu_s t_s - \mu_F t_F) \tag{C2}$$

where I_{sF} is the transmitted intensity through both the filter and the sample, μ_F is the absorption coefficient of the filter and t_F is the thickness of the filter. Equation C2 may be rewritten as

$$I_{sF} = I_o T_s T_F \tag{C3}$$

where $T_F = \exp(-\mu_F t_F)$ and T_s has already been defined.

The sample is then lowered out of the beam and the intensity of the transmitted beam through only the filter is measured. The equation which relates the incident intensity to the transmitted one is:

$$I_F = I_o T_F \tag{C4}$$

where I_F is the intensity of the transmitted beam through only the filter.

If Equations C4, C3, and C1 are combined, then the incident intensity is related to the three transmitted intensities by

$$I_o = \frac{I_F I_s}{I_{sF}} . \tag{C5}$$

The filters used in this study were nickel and zirconium foils. All samples and filters were between the scattering and receiving collimators. Since only an estimate was required, air scattering and scattering due to the filter was not accounted for. The method described was used to estimate I_o for the fundamental as well as the harmonic wavelengths.

For the silicon and germanium data, both filters were used separately along with each sample crystal. The final estimate for the incident intensity was determined by averaging the incident intensities obtained by each filter. For the HOPG crystal which was not in the closed-cycle refrigerator, only a nickel filter was used since it was

the only one available at that time. The HOPG crystal in the refrigerator presented a different problem. Since the sample crystal and refrigerator head could not be easily removed from the beam an adaptation of the above method was used.

Instead of moving the refrigerator head and the HOPG crystal, another crystal was used as the sample crystal and the refrigerator head remained in the beam. The additional scattering due to air, crystal or refrigerator head was not accounted for in this estimate. Both the nickel and zirconium foils were used separately along with a sample silicon crystal to obtain incident intensities. The intensities derived from the data of each foil were averaged and this average was used for the estimated incident intensity.

The nice aspect of this method is that neither the thicknesses nor the absorption coefficients of the sample or foils need be known. The only requirements are that the relative thickness of the crystal and filter with respect to the beam be constant. Also, the crystal or filter must not be a material which will fluoresce near the wavelength chosen to estimate I_o. There are, of course, other more accurate methods available to measure I_o such as multiple foils (Batterman et al., 1961) or reflections from Aluminum powder (Schwartz and Cohen, 1977). For the purposes of this study, however, accurate determination of the incident intensity was not needed since it could be determined directly from the raw data through least-squares fitting. The estimates of I_o obtained in this method was sufficient for use as an initial parameter in the fitting program NLS.